Amplification-Free, High-throughput Nanoplasmonic Quantification of Circulating microRNAs in Unprocessed Plasma Microsamples for Earlier Pancreatic Cancer Detection

Adrianna N. Masterson,[1] Nayela N. Chowdhury,[2,3] Yue Yang,[4] Michele T. Yip-Schneider,[5] Sumon Hati,[1] Prashant Gupta,[6] Sha Cao,[4] Huangbing Wu,[5] C. Max Schmidt,[3,5] Melissa L. Fishel,[2,3,7] and Rajesh Sardar[1,3,*]

[1]Department of Chemistry and Chemical Biology, Indiana University-Purdue University Indianapolis, Indiana 46202, United States

[2]Indiana University School of Medicine, Department of Pediatrics, Wells Center for Pediatric Research, Indianapolis, Indiana 46202, United States

[3]Indiana University Melvin and Bren Simon Comprehensive Cancer Center, Indianapolis, Indiana 46202, United States

[4]Department of Biostatistics and Health Data Science, Indiana University School of Medicine, Indianapolis, Indiana 46202, United States

[5]Department of Surgery, Indiana University School of Medicine, Indianapolis, Indiana 46202, United States

[6]Department of Mechanical Engineering, Washington University, St. Louis, Missouri 63130, United States

[7]Indiana University School of Medicine, Department of Pharmacology and Toxicology, Indianapolis, Indiana 46202, United States

***Corresponding author email: rsardar@iupui.edu**

Abstract

Pancreatic ductal adenocarcinoma (PDAC) is a deadly malignancy often detected at an advanced stage. Earlier diagnosis of PDAC is key to reducing mortality. Circulating biomarkers such as microRNAs are gaining interest, but existing technologies require large sample volumes, amplification steps, and extensive biofluid processing, lack sensitivity, and are low-throughput. Here, we present an advanced nanoplasmonic sensor for highly sensitive, amplification-free detection and quantification of microRNAs (microRNA-10b, -let7a) from unprocessed plasma microsamples. The sensor construct utilizes uniquely-designed -ssDNA receptors attached to gold triangular nanoprisms, which display unique localized surface plasmon resonance (LSPR) properties, in a multi-well plate format. The formation of -ssDNA/microRNA duplex controls the nanostructure-biomolecule interfacial electronic interactions to promote the charge transfer/exciton delocalization processes and enhance the LSPR responses to achieve attomolar (10^{-18} M) limit of detection (LOD) in human plasma. This improve LOD allows the fabrication of high-throughput assay in a 384 well plate format. The performance of nanoplasmonic sensors for microRNA detection was further assessed by comparing with qRT-PCR assay of 15 PDAC patient plasma samples that shows a positive correlation between these two assays with the Pearson correlation coefficient value >0.86. Evaluation of >170 clinical samples reveal that oncogenic microRNA-10b and tumor suppressor microRNA-let7a levels can individually differentiate PDAC from chronic pancreatitis and normal controls with >94% sensitivity and >94% specificity at 95% confidence interval (CI). Furthermore, combining both oncogenic and tumor suppressor microRNA levels significantly improve to differentiate PDAC stages I & II versus III & IV with >91% and 87% sensitivity and specificity, respectively, in comparison to the sensitivity and specificity values for individual microRNAs. Moreover, we show the that the level of microRNAs varies substantially in pre- and post surgery PDAC patients (n = 75). Taken together, this ultrasensitive nanoplasmonic sensor with excellent sensitivity and specificity is capable of assaying multiple biomarkers simultaneously and may facilitate early detection of PDAC to improve patient care.

Keywords: localized surface plasmon resonance, nanoplasmonic sensor, interfacial charge transfer, high-throughput assay, microRNA, unprocessed plasma, pancreatic cancer, early detection

Pancreatic ductal adenocarcinoma (PDAC), commonly known as pancreatic cancer, is a deadly malignancy with a 11% five-year survival rate.[1] PDAC symptoms are vague, such that 80-85% of patients are diagnosed at later stages when the cancer has invaded surrounding vessels and metastasized.[2, 3] Resection of small, localized and potentially curable tumors improves the 5-year PDAC survival rate to ~60%.[4-7] PDAC is predicted to be the second leading cause of cancer-related death by 2030;7 therefore, there is an urgent and unmet clinical need for more reliable detection technology for screening and diagnostic purposes to reduce mortality. Additionally, other gastrointestinal conditions such as chronic pancreatitis (CP) can confer increased risk for developing PDAC, emphasizing the importance of early detection in high risk patient populations.[8]

Lack of reliable blood markers capable of early PDAC detection reduces potential screening effectiveness. Currently, the blood marker carbohydrate antigen 19-9 (CA19-9) is used for treatment monitoring of PDAC with <76% and 78% sensitivity and specificity, respectively, at 95% confidence interval (CI).[9] To increase patient survival and achieve cost effectiveness, a minimum of 88% biomarker sensitivity and 85% specificity are required.[10] Furthermore, CA19-9 is not specific for PDAC because an elevated level may be associated with CP.[11] Moreover, ~15% of PDAC patients are Lewis blood group negative, therefore lacking the ability to produce detectable levels of CA19-9.[11, 12] Together, it is an unreliable biomarker for early PDAC detection. To obviate these current challenges, liquid biopsies are being developed for circulating tumor DNAs,[13, 14] microRNAs,[15-18] proteins,[19, 20] tumor cells,[21, 22] and extracellular vesicles[23, 24] for earlier detection of PDAC. These advanced techniques possess inherent challenges such as low specificity and sensitivity and the lack of high-throughput capability, limiting their utility in population-based translational research and in the clinical setting. Therefore, it is of paramount importance to develop a simple but ultrasensitive and highly selective technology that can detect and quantify multiple biomarkers in larger patient cohorts.

MicroRNAs are small single stranded, non-coding RNAs consisting of 18-25 nucleotides that play major roles in cell proliferation, survival, migration, invasion, and metastasis in various cancers.[25-27] They are present in the blood circulation and are remarkably stable in plasma and/or serum, and resistant to RNase activities.[28, 29] Furthermore, microRNAs are also stable for multiple numbers of freeze-thaw cycles.[30] Additionally, their variable expression levels in blood plasma can differentiate PDAC from healthy individuals (normal control, NC).[31] Reverse transcriptase-polymerase chain reaction (RT-PCR), DNA microarrays, and sequencing technologies are widely used microRNA assay techniques. The clinical utility of these techniques is hampered by three practical challenges: ***(i)*** requirement of large sample volume; ***(ii)*** time-consuming RNA/DNA isolation form biofluids, followed by further amplification; ***(iii)*** inadequate assay sensitivity,

specificity, and accuracy for low-abundance biomarkers.[32] Fluorescence-33, colorimetric-34, and electrochemical-based35, 36 capture probes can assay microRNAs without amplification and/or extraction process for clinical diagnosis, however these techniques require large sample volume, lack high-throughput capabilities, and/or display insufficient sensitivity and specificity required in the clinical setting.[37]

To address the shortcomings of these existing approaches, here, we report the development of an amplification-free and label-free, solid-state nanoplasmonic sensor for high-throughput analysis of unprocessed clinical plasma samples. We utilized the unique localized surface plasmon resonance (LSPR) property of gold triangular nanoprisms (Au TNPs) covalently attached onto the glass-bottom of a 384 well-plate. The first LSPR-based biosensor had constructed nearly three decades ago,[38, 39] however, to the best our knowledge, this label-free sensing approach has yet to be implemented in a 384 well format to prepare an LSPR-based, solid-state detection technology capable of performing high-throughput assay in real-world samples. Although biosensing based on photonic crystals and resonant waveguide, while utilizing 384 microplates were developed,40, 41 to the best of our knowledge, this is the first LSPR-based approach utilizing a 384 well-plate format. The fundamental working principle of this plasmonic-based technology is based on an LSPR spectra shift of -ssDNA-modified Au TNPs upon hybridization with microRNAs.[42, 43] Herein, we show a new approach of enhancing the LSPR sensitivity where modification of -ssDNA with programmably selected organic ligands markedly enhanced the sensitivity (attomolar range) as a consequence of increased charge transfer at the nanostructure-biomolecule interface in solid-state.

Uniquely, our nanoplasmonic sensors demonstrate excellent sensitivity and specificity of the microRNA markers in cohorts of individuals without pancreatic disease (NC, n=60), with CP (n=35) and with PDAC (n=90, stage I-IV cancer) from blood plasma samples. Although, large cohort studies involving qRT-PCR-based assay of circulating microRNAs for early detection of pancreatic cancer have been conducted,44, 45 to the best of our knowledge, this the largest cohort study has been reported where microRNAs are detected and quantified using label- and amplification-free detection approach. The sensitivity and specificity of the combined biomarkers for differentiating between PDAC stage I & II versus CP and PDAC stage I & II versus III & IV markedly improve compared to each microRNA alone. Our results are a significant advancement in earlier PDAC detection because qRT-PCR-based plasma assay demonstrated that either microRNA-10b or -let7a can differentiate PDAC from normal control, but they are not able to distinguish different stages of PDAC.[44] Moreover, the microRNA expression levels in matching pre- and post-surgery PDAC plasma samples show striking differences, further confirming their

specific association with PDAC and suggesting potential tumorigenic roles. Our results demonstrate that this amplification-free, high-throughput method detecting and quantified microRNAs in microplasma samples can be used in clinical diagnostic setting not only for PDAC but also for a wide range of cancers and other diseases.

Results

Development of a high-throughput nanoplasmonic sensor for microRNA assay. When light interacts with metal nanoparticles (MNPs), the incident electric field drives the collective oscillation of their conduction electrons known as localized surface plasmon resonances (LSPRs). The LSPR-active MNPs are considered as nanoantennas because they can transfer and condense far-field electromagnetic (EM) energy into near-field "hot-spots" at the surface of MNPs. Thus, the LSPR and EM both depend on MNP size and shape, and their local dielectric environment.[38, 39] Recently, we reported the fabrication of a nanoplasmonic sensor in a 96-well format for highly selective microRNA detection and quantification from 10 μL cancer patient plasma samples with attomolar (aM, 10^{-18} M) limit of detection (LOD, defined as mean of blank + 3 σ, σ = standard deviation of blank) where an individual well can be considered as a single nanoplasmonic sensor. Utilizing the basic designer approach, we further improved the fabrication strategy to construct the first plasmonic-based biosensors in a 384-well format (**Figure 1a**). The nanoplasmonic sensor fabrication involved two steps (**Figure 1b**): (i) chemical attachment of colloidally-synthesized, ~42 or 55 nm edge-length Au TNPs onto mercaptomethoxysilane-modified glass substrate (**Figure 1c,d and Supporting Figure 1,** a detailed description of the nanoplasmonic sensor fabrication is provided in the Method Section); (ii) covalent functionalization of TNP surface with a mixture of thiolated single-stranded DNA (-S-$(CH_2)_3$-ssDNA) as a receptor and polyethylene glycol thiolate (-S-PEG_4) as a spacer. The -S-PEG_4 also served as blocking agents to reduce fouling effects, which is defined as competing adsorption of unwanted biomolecules at the surface of MNPs.[46] Au TNPs are special nanoantennas with excellent LSPR properties. The finite-difference time-domain (FDTD) simulation showed near-field enhancement at sharp corners and edges that together increases the sensitivity (**Figure 1e,f**).[47, 48] Their atomically flat surface, which allows the formation of uniform self-assembled monolayers (SAM) of receptor and spacer molecules to reduce unwanted adsorption of biomolecules onto the surface of Au TNPs from human biofluids. Gold-thiolate (Au-S-) bonds are highly stable, which is also important for long-term stability and reproducibility of the nanoplasmonic sensor. Finally, depending on the edge-length, colloidal solutions of our synthesized Au TNPs display an LSPR dipole peak (λ_{LSPR}) in the 750-850 nm region (**Supporting Figure 2**) which is important to avoid spectra interference from water

adsorption, specifically crucial for biosensing applications.[49] The nanoplasmonic sensing mechanism involves direct hybridization between -ssDNAs and target microRNAs to form a DNA/RNA duplex, which increases the refractive index around the TNPs and facilitates delocalization of plasmon excitons[50], that together influence the λ_{LSPR} position by shifting it to longer wavelengths (red shifts) in a 384-well format (**Supporting Figure 3**). The nanoplasmonic sensor in a 384-well format was utilized to assay microRNA-10b and the LOD, calculated from the total LSPR shift ($\Delta\lambda_{LSPR} = \lambda_{LSPR,\ microRNA} - \lambda_{LSPR,\ ssDNA}$) versus the microRNA concentration, was calculated to be 2.5 femtomolar (fM, 10^{-15} M) (**Figure 1h, Supporting Figure 4, Table S2**). We also calculated the limit of quantification (LOQ) for each system, and the values are provided in **Table S2**.

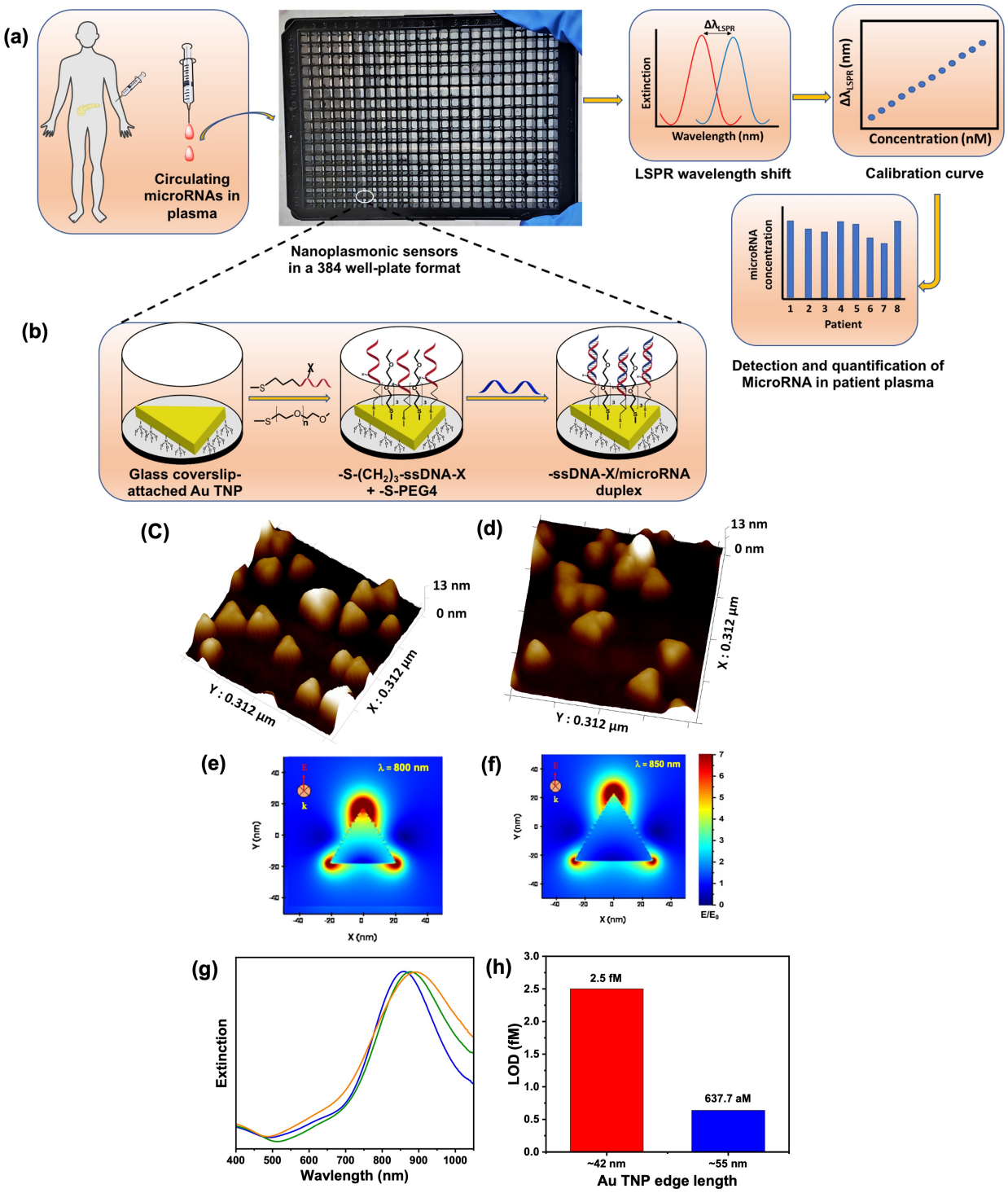

Figure 1. Fabrication of a high-throughput nanoplasmonic sensing platform for microRNA detection and quantification. (a,b) Schematic showing the fabrication of nanoplasmonic sensing platform where microRNA attachment to individual sensor and formation of –ssDNA/microRNA duplex causes an LSPR (spectra) shift, which is measured to quantify the amount of microRNAs present in the patient biospecimens. (**c,d**) Atomic force microscopy images of 42 and 55 nm edge length Au TNPs. Electric (E/E_0) near-field patterns generated using FDTD calculations of **(e)** 42 and **(f)** 55 nm edge-length Au TNPs. **(g)** UV-vis extinction spectra of silanized glass substrate-attached 55 nm edge length Au TNPs (blue curve, 859.1

nm), after -S–$(CH_2)_3$-ssDNA-10b- and –S-PEG_4 functionalization (green curve, 882.1 nm), and after incubation in a 100 nM microRNA-10b solution (orange curve, 893.1 nm). (**h)** Limit of detection calculated from an average $\Delta\lambda_{LSPR}$ of six measurements for microRNA-10b assay utilizing 42 and 55 nm edge length Au TNPs.

The LOD for the 384 well-plate is nearly three orders of magnitude higher than the nanoplasmonic sensor previously constructed with a 96-well plate,[51] which could be due in part to a lower number of microRNAs in the small sample volume, total 120 and 300 μL for 384- and 96- well, respectively, and a smaller nanoplasmonic sensor area. To achieve our first goal towards analyzing microRNAs in microliter biofluids, particularly for tumor suppressor microRNAs, it is extremely important to improve the assay sensitivity. Therefore, we used ~55 nm edge-length Au TNPs in the current sensor fabrication which resulted in an LOD of 637.7 aM (LOQ = 45 fM) for microRNA-10b (**Figure 1c-h, Supporting Figure S1, Supporting Figure 4A and Table S2**). A large sensing volume and a much red-shifted λ_{LSPR} (~850 nm in acetonitrile) of 55 nm edge-length in comparison to 42 nm (~800 nm in acetonitrile) edge-length TNPs are expected to improve the sensitivity of nanoplasmonic sensors.[52-54]

Enhancement of nanoplasmonic sensor performance for PDAC-associated microRNA analysis. Our overarching goal is to differentiate different pancreatic diseases and achieve early pancreatic cancer detection utilizing a few microliters of patient biofluids from a large cohort of samples. There is an unmet need to analyze low abundance microRNAs which may be present at the disease onset, while maintaining high-throughput capabilities; therefore, improving the sensitivity of the 384 well-plate nanoplasmonic sensor further is a prerequisite. Increasing the edge-length of TNPs further should improve the sensitivity, however, that would move λ_{LSPR} towards 900-1000 nm region, leading to spectral interference and increasing false responses. To mitigate such issues while further improving the LOD, we kept TNP edge-length (~55 nm) constant but modified the structure of -ssDNA. In the LSPR-based analyte detection, the sensing mechanism exclusively relied on the change in local refractive index.[55, 56] We believe that for the microRNA assay, interfacial electronic states between the MNP and attached biomolecules would play crucial roles to allow charge delocalization,[50] similar to DNA-mediated charge transport,[57] and to improve sensitivity. Therefore, we tested the hypothesis that appropriate interfacial dipole moment would facilitate the transfer of Au TNP electrons in to highly conjugated π-system of -ssDNA/microRNA duplex, resulting in the modulation of the free electron density and thus shifting of LSPR peak position. It is known that red-shifting of the LSPR peak of MNPs leads to an increase of biosensing sensitivity.[39, 49] The proposed charge transfer mechanism, known as

chemical interference damping (CID)[58] allows transfer of electrons from MNPs in to the interfacial electronic states that are formed upon formation of MNP-surface ligand conjugates. According to Drude-Lorentz model, transfer of MNP electrons will reduce the overall free electron density of Au resulting in a red shift the LSPR peak.[39] Together, the CID effect is controlled by the magnitude of TNP-ssDNA/microRNA duplex interfacial dipole where a higher interfacial dipole results in better charge transfer and larger LSPR response.[59] We studied this working mechanism by modifying the -ssDNA backbone, specifically the first thymine nucleic acid present on the 3' end of the sequence, with Amino-T and Super-T (**Figure 2a**). Importantly, attachment of Amino-T and Super-T to Au TNPs produced λ_{LSPR} of ~886 and 892 nm, respectively. The λ_{LSPR} significantly red-shifted in comparison to -S–$(CH_2)_3$-ssDNA-10b-functionalized (without modification) Au TNPs (λ_{LSPR} = 882 nm).

The LODs of microRNA-10b assays for Amino and Super-T modified -ssDNA-10b receptor were determined to be 381.9 and 83.5 aM, respectively (**Figure 2b,c** and **Table S3**). The calculated LOQ for each system, and the values are provided in **Table S3.** The sub-femtomolar detection limit and negligible background response justify our nanoplasmonic sensor as *"highly sensitive bioanalytical sensor."*[60] With the LOD of ~84 aM in PBS buffer, a 10 μL sample would contain approximately 500 microRNAs. This result is highly intriguing in terms of number of microRNAs that can be quantified in a small sample volume but is not unique in terms of detection and quantification capability. Utilizing surface plasmon resonance (SPR) sensors constructed with gold nanorods, Xue et al., reported LOD of 10 aM where ~30 microRNAs were detected from 5 μL sample volume.[61] Wang and coworkers reported LOD of 100 aM from the LSPR-based detection of microRNAs.[62] Few other LSPR-based nucleic acid detection methods reported LODs 1-5 pM,[63-65] which ~10^5 lower than our most improved value of ~84 aM. It is important to mention that all previously reported methods failed to demonstrate the clinical applicability of constructed sensors by analyzing real-world samples, which has been carried out as part of this current work. As shown in Figure 2b, our calibration curve provided linearity of eleven order of magnitude ranging 10 aM to 100 nM in the logarithmic scale. This extremely large range of linearity is not too surprising considering previously reported,[61, 66, 67] plasmonic-based sensors can display linear dynamic range of 7 to 11 order of magnitudes within the concentration rage of 100 nM to 1 aM. Perhaps, unique structural and LSPR properties of plasmonic nanostructures are capable of providing such a large linearity where diffusion kinetics at an extremely low concentration and supersaturation at a moderately concentration (in nM) can be avoided. Together, Super T thymine modified -ssDNA-10b resulted in a 7-fold improvement in LOD compared to the unmodified thymine base. Finally, we determined the binding dissociation

constant (K_d) of -ssDNA/microRNA using a Langmuir isotherm (see Figure S4B) at room temperature.68 The calculated K_d value of 1.50 x 10^{-9} M is in good agreement with the literature.69, 70 Together, the data further strengthens the validation of our developed calibration curves. It is important to mention that the -ssDNA/microRNA hybridization with ~20 base-pair does not fully follow the Langmuir isotherm model because most adsorption experiments were conducted at room temperature, which is lower than the DNA melting temperature, along with other factors such as solution pH and ionic strength together can influence to achieve complete dehybridization of the -ssDNA/microRNA duplex. We plan to investigate this in the future utilizing our LSPR-based approach.

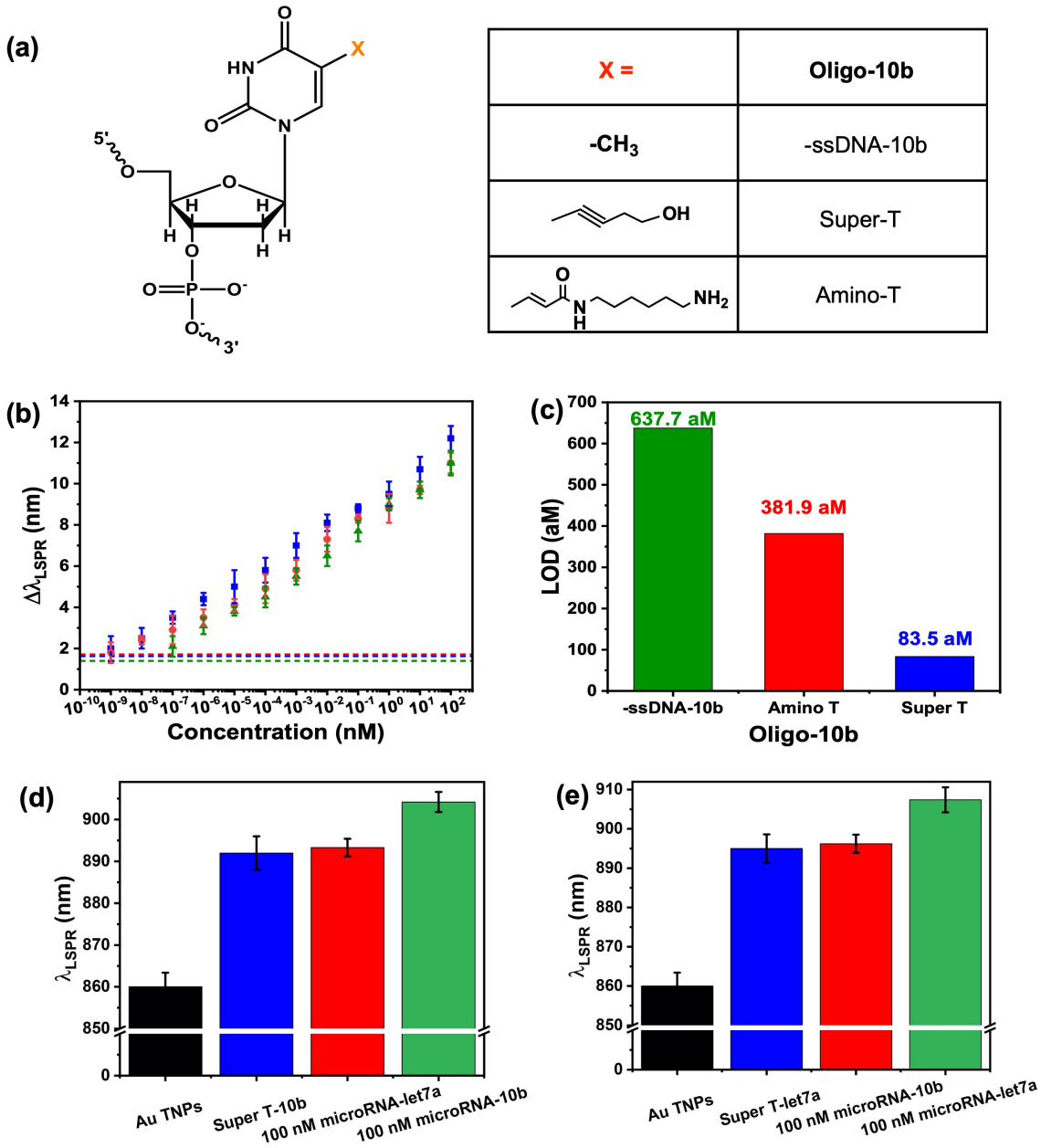

Figure 2. Characterization of the performance of high-throughput nanoplasmonic-based assay with microRNAs. **(a)** Structure of sugar ring-attached thymine base in the –ssDNA receptor with different chemical modifications (X). The figure chemical structure was prepared using ChemDraw Professional 17.0 software. (**b)** Shift in λ_{LSPR} peak position ($\Delta\lambda_{LSPR}$) of nanoplasmonic sensors as a function of microRNA-10b concentrations (100 nM to 1 aM) in PBS buffer utilizing –ssDNA-10b (green triangles), Amino-T (red circles), and Super-T (blue squares) as the receptor molecule. The dotted lines represent blank values obtained from the average of six measurements. (**c)** Calculated limit of detections for microRNA-10b assay as a function of receptor molecules *i.e.,* –ssDNA-10b, Amino-T, and Super-T. (**d)** Specificity test of microRNA-10b sensors constructed with 55 nm edge length Au TNPs during different stages of surface modification: as synthesized TNPs, after -S–$(CH_2)_3$-ssDNA-Super T-10b- and –S-PEG_4 functionalization, after incubation in 100 nM microRNA-let7a, and after incubation in 100 nM microRNA-10b. (**e)** Specificity test of microRNA-let7a under similar experimental conditions as described in (d). Data in (b,c), and (d) are mean± s.d., n=6 repeated measurements. To examine nonspecific interactions of unwanted biomolecules

with nanoplasmonic sensors at lower concentrations, it was plotted on the axis in logarithm scale. The log scale is commonly used in the LSPR-based biosensing.[71, 72]

To support our experimental data, we performed density functional theory (DFT) calculations[73] to determine the induced surface dipole moment on metal (μ_{metal}) for each -ssDNA fragments and then subtracting the total dipole moment (μ_{total}) by the gas-phase dipole moment (μ_{ads}) of the molecule (adsorbate). DFT calculations were performed on -ssDNA structures with first 3 nucleotides (G-T-A) in a deoxyribose sugar backbone next to the linker (O-CH_2-CH_2-CH_2-SH), **Figure S5**. Calculated dipole moments for each -ssDNA structure attached to an Au atom ("Total Dipole Moment") and in the gas-phase without presence of any Au atoms ("Gas-Phase Thiol Dipole Moment"), and the resulting induced dipole moments of the Au surface ("Au Surface Induced Dipole Moment") are listed in **Table S4**. The results of the computational calculations revealed that an Au atom modified with –ss-DNA-10b and SuperT and AminoT in a thymine residue exhibited different surface induced dipole interactions. SuperT induced higher dipole moment on the Au surface (μ_{metal}) (15.3116 D) followed by AminoT (3.1807 D), and finally –ss-DNA-10b exhibited the lowest Au-surface induced dipole moment (1.3162 D). These values support our hypothesis that as SuperT has the highest Au-surface induced dipole moment (μ_{metal}), in response the freely moving fermi level electrons will create the highest number of image dipoles in plasmonic Au TNP-ligand interface generating additional scattering centers for plasmon dephasing showing the highest CID effect, the largest LSPR response and the best LOD for SuperT/Au system.

With the knowledge that utilizing larger Au TNPs (~55 nm edge length) and a Super-T modified thymine nucleic acid base in the -ssDNA receptor sequence provides a much-improved limit of detection, we performed microRNA assays in 10% human plasma for PDAC-specific microRNAs. MicroRNA-10b and microRNA-let7a assays were performed utilizing 100 nM-1 aM microRNA in 10% human plasma (**Supporting Figure 6**) and LODs of 133.3 aM and 129.4 aM, respectively, were obtained (**Table S5**). Next, the specificity of the biosensor platform was explored. The successful implementation of any biosensors for disease diagnosis requires examination of their specificity of target microRNAs in real biological samples. We tested the specificity of nanoplasmonic sensor by functionalizing Au TNPs with mixed S–$(CH_2)_3$-ssDNA-Super T-10b- and –S-PEG_4 functionalization. This sensor is very specific to microRNA-10b detection. Upon incubation in the non-complementary microRNA, i.e., microRNA-let7a prepared in 10% human plasma, a negligible LSPR dipole peak red shift (<2.0 nm) occurred (**Figure 2d**). A similar specificity test was conducted for microRNA-let7a (**Figure 2e**). The small red shift could be due to instrumental or background noise. Our result is in agreement with Zhang et al., who reported

~1.5 nm LSPR shift in serum for a single nucleotide mismatch for microRNA detection utilizing a nanoplasmonic sensor constructed with Au nanocubes.[63] Additionally, they developed calibration plot of microRNAs in logarithm concentration scale by accepting LSPR shifts as low as 0.9 nm in determining the LOD of 5 pM in serum. Nevertheless, the high specificity of our nanoplasmonic sensor appears due to the non-fouling effect of PEG which prevents nonspecific adsorption of unwanted extraneous biomolecules present in human plasma. Furthermore, high sensitivity of our nanoplasmonic sensor allows measurements to be conducted in 10X diluted human plasma, thus improving the specificity by avoiding the interaction and adsorption of non-complementary microRNAs and/or proteins. We calculated the coefficient of variance (CV) for the concentration dependent LSPR shifts in plasma (See Figure S6) and found to <10% for microRNA concentrations up to 1.0 fM, whereas ~15% CV value was obtained for 100 and 1.0 aM concentrations. Overall, our bioanalytical sensor provided a high sensitivity and specificity, indicating that it could be used for highly sensitive and specific PDAC disease diagnosis and monitoring in patient samples.

Performance and accuracy of nanoplasmonic sensors in biofluid-derived, pancreatic cancer-associated microRNA assay. Overexpressed microRNA-10b leads to tumor progression, invasion, and metastasis in human PDAC,[74, 75] whereas the loss of microRNA-let7a, downregulated in PDAC, correlates with tumor transformation.[76] Analysis of archival plasma samples showed overexpression and down-regulation of microRNA-10 and -let7a, respectively, in PDAC compared to healthy individuals (normal control, NC).[77] In the first validation of our nanoplasmonic sensor performance in real biofluids, we assessed microRNA-10b levels in conditioned media from human pancreatic cancer cells (Pa03C), to quantitate microRNA-10b from monolayer (2D)- and three-dimensional (3D) spheroid cultures. We specifically selected the 3D cell growth model because it closely resembles actual tumor growth microenvironments.[78] Nanoplasmonic sensors were incubated in the diluted conditioned media overnight (~12-14 hr), and then rinsed with PBS buffer, following by acquisition of LSPR spectra. The calculated concentrations fall below the LOD, therefore, microRNAs could be detected but were not quantifiable on Day-1. The concentration steadily increased over time without any linear trend (**Figure 3a,b**). MicroRNA levels in the 2D- and 3D-conditioned media cannot be directly compared because the number of cells and growth conditions were not identical. We were also able to detect minute concentrations of microRNA-let7a at the last timepoint of the conditioned media experiments when cell number was the highest (**Supporting Figure7**).

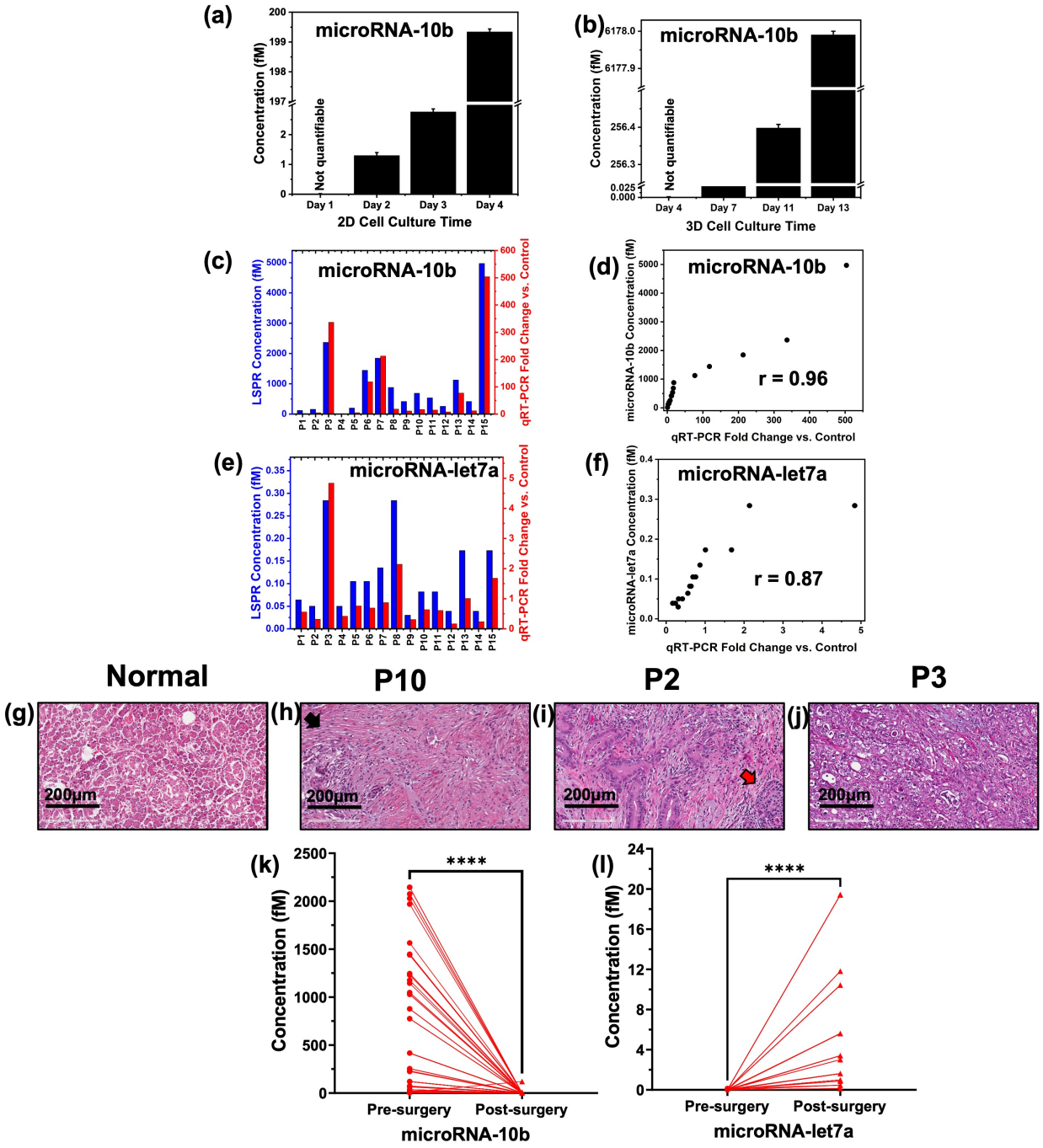

Figure 3. Performance evaluation of nanoplasmonic sensors by detecting microRNAs in cell conditioned media and PDAC patient plasma samples. microRNA-10b (black bars) quantification from PDAC cell lines (**a**) Conditioned media from 2D cultures and (**b**) 3D spheroids cultures of Pa03C cells. Data in **a,b** are mean± s.d., n=3 triplicate samples per time point. Some concentration values fall below the LOD of ~130 aM, therefore the level of microRNAs is considered to only be detected and not quantified. **c-f**, Direct comparison of microRNA-10b (**c**) and microRNA-let7a (**e**) assays and correlation graphs (**d, f**) obtained through gold standard PCR (red) and LSPR-based (blue) biosensing platform in 15 PDAC patient samples (validation cohort). The "r" is the Pearson correlation coefficient. H&E-stained section of normal pancreas (**g**) and PDAC patients (**h-j**) with black arrow showing anaplastic ducts surrounding the stroma

and black/red arrow showing Islet of Langerhans. microRNA-10b (**k**) and microRNA-let7a (**l**) concentrations assayed from 75 PDAC patient pre- and and post-surgery plasma samples (study cohort). P values were determined by Wilcoxon paired t-test. ****P < 0.0001. Data in **k,l** are mean± s.d., n=2 duplicate per sample. Researchers performing the PCR and LSPR analyses were blinded to sample identity.

Development of any new disease diagnostic technology requires validation with FDA-approved "gold standard" techniques. Therefore, we performed a blinded assay of 15 PDAC patient plasma samples as a validation cohort. The qRT-PCR-based microRNA-10b and -let7a fold change versus internal controls is in excellent agreement with concentrations determined using nanoplasmonic sensor, as demonstrated by strong positive correlation between the qRT-PCR and nanoplasmonic assays with r values of 0.96 and 0.87 for microRNA-10b and -let7a, respectively (**Figure 3c-f)**. In comparison to normal pancreas (**Figure 3g**), three of the tumors from the patients in the validation cohort are shown after H&E staining (**Figure 3h-j**). Patient 10 has Stage II PDAC and the anaplastic ducts surrounded by stroma are indicated by the black arrow (**Figure 3h**). Patients 2 and 3 have Stage III PDAC with P2 demonstrating scattered ductal adenocarcinoma with ducts of varying size surrounded by large areas of tumor stroma and an area with an Islet of Langerhans (**Figure 3i, black/red arrow**). P3 had minimal stroma between the tumor tissue, also anaplastic ductal adenocarcinoma and the tumor cells are poorly differentiated (**Figure 3j**). P3 had one of the highest levels of microRNA-10b and P2 had one of the lowest levels of microRNA-let7A as determined by both qRT-PCR and the nanoplasmonic sensor. The concentration of microRNA-let7a (Figure 3e), microRNA10b in post-surgery samples (Figure 3k), and microRNA-let7a in pre-surgery samples (Figure 3l) appeared to be below the LOD value (~130 aM in plasma). In clinical viewpoint, under such circumstances, we must consider that analytes (microRNAs) can only be detected but are not precisely quantifiable.

Finally, plasma samples obtained from 75 PDAC patients before (pre-surgery) and after (post-surgery) pancreas resection were analyzed to evaluate the clinical screening applicability of our nanoplasmonic sensors in terms of microRNA-10b and -let7a levels and their specificity for PDAC detection. We followed the same incubation time as described for the cell conditioned media. For microRNA-10b, concentrations were in the 2.9-2076 fM range in pre-surgery PDAC plasma and significantly decreased 3-5 days post-resection (p <0.0001) (**Figure 3k**, **Supporting Figure 8)**. All the patients exhibited low plasma microRNA-10b levels post operatively. In contrast, plasma microRNA-let7a levels were exceedingly low in pre-surgery PDAC patient plasma samples and increased significantly after surgery (**Figure 3l, Supporting Figure 8**). There were no significant differences in microRNA-10b and -let7a levels between male and female patients (**Supporting Figure 9)**. Analysis of these pre- and post-surgery plasma samples from the same patient is especially informative as observed differences in biomarker levels may be associated

with the presence/absence of the tumor rather than patient-to-patient variation. Thus, the differential expression of microRNA-10b and -let7a in pre- versus post-surgery plasma identifies them as promising clinically relevant PDAC-associated biomarkers.

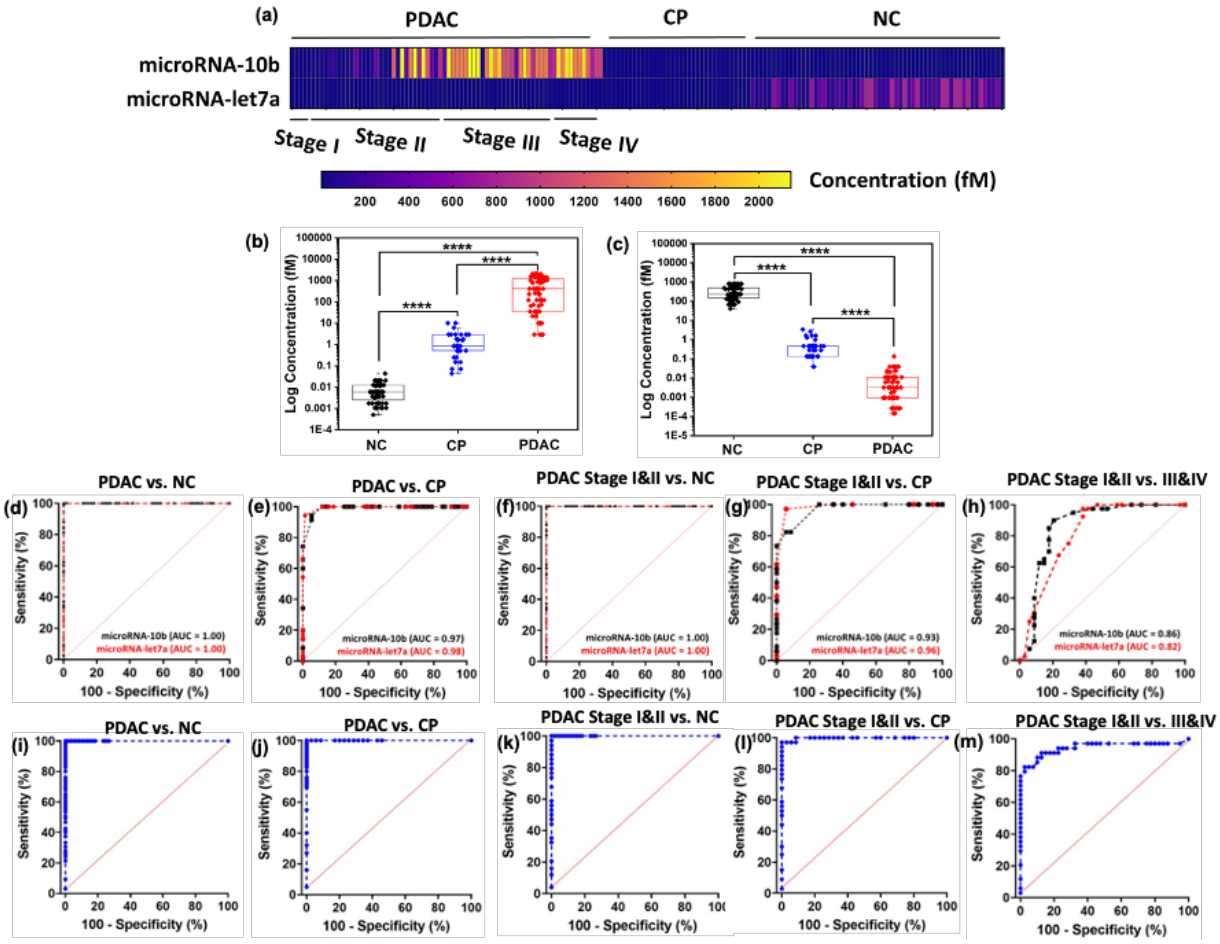

Figure 4. MicroRNA signature differentiation of pre-surgery PDAC patients from chronic pancreatitis and normal control group in the study cohort. (a) Comparison of microRNA-10b and -let7a levels in plasma samples of PDAC (n=75: 5 stage I, 29 stage II, 29 stage III, and 11 stage IV), CP (n=35), and NC (n= 60). (**b,c)** The established microRNA-10b (**b**) and microRNA-let7a (**c**) concentrations measured in 75 PDAC, 35 CP and 60 NC patient plasma samples showed 100% accuracy between three different groups. Pairwise comparison P values were determined by one-way ANOVA. ****P < 0.0001. (**d-h)** Receiver operating characteristic (ROC) curves of individual plasma microRNA-10b (black squares) and microRNA-let7a (red circles) levels distinguishing PDAC pre-surgery from NC (**d**), PDAC pre-surgery from CP (**e**), PDAC pre-surgery stage I&II from NC (**f**), PDAC pre-surgery stage I&II from CP (**g**), and PDAC pre-surgery stage I&II verses Stage III&IV (**h**). ROC curves obtained by combining microRNA-10b and microRNA-let7a levels to differentiate PDAC pre-surgery from NC (**i**), PDAC pre-surgery from CP (**j**), PDAC pre-surgery stage I&II from NC (**k**), PDAC pre-surgery stage I&II from CP (**l**), and PDAC pre-surgery stage I&II verses Stage III&IV (m). ROC area under the curve (AUC) values distinguishing different diseases states and conditions for each group are summarized in Table 2.

High-throughput nanoplasmonic-based microRNA assay for early PDAC diagnosis. Further assessment of our nanoplasmonic sensors for clinical cancer diagnostics was conducted by analyzing microRNA-10b and -let7a in 35 CP and 60 NC plasma samples in a short analysis time. Our selected 75 PDAC cohort contained 45% stages I & II patients with remaining patients at stages III & IV (**Table 1**). The total of 170 patient plasma samples in our cohort is substantially higher than the capacity of other nanotechnology-based optical assays for PDAC diagnosis characterizing similar types of patient samples.[23, 24] The analysis of a large cohort is feasible because of the high-throughput assay capability of our developed sensors. MicroRNA-10b levels were significantly higher in late-stage (stages III & IV) than early-stage (stages I & II) PDAC, whereas microRNA-let7a levels were lower in late-stage versus early-stage PDAC (**Figure 4a and Supporting Figure 10**). As illustrated in **Figure 4b,c,** and **Supporting Figure 11** each microRNA was able to differentiate between PDAC, CP and NC groups with $p < 0.0001$. Each microRNA provided 100% sensitivity and 98% specificity for PDAC versus NC (**Figure 4d, Table 2**). The nanoplasmonic sensor-based microRNA assay demonstrated excellent discriminating power between PDAC and CP (94% sensitivity) compared to CA19-9 (<42% sensitivity at 95% CI) (**Figure 4e, Table 2, Supporting Figure 12**). Although concentrations of microRNA-10b/let7a showed up below the LOD value (~130 aM), the data presented herein are highly valuable and can be used to distinguish between different pancreatic pathology.

Further analysis by stage revealed excellent sensitivity (100%) for microRNA-10b and -let7a in discriminating early stage PDAC versus NC (**Figure 4f**). MicroRNA-let7a displayed improved sensitivity (97%) compared to microRNA-10b (82%) in differentiating early stage PDAC versus CP (**Figure 4g**). In contrast, CA19-9 showed only 29% sensitivity in distinguishing between the latter group of patients (**Table 2**). Interestingly, although microRNA-10b and microRNA-let7a were each capable of differentiating between early- and late-stage PDAC, significantly better than CA19-9 (**Figure 4h, Table 2, Supporting Figure 13 &14),** relatively low sensitivity (62-67%) was observed for each individual microRNA, suggesting lower performance in discriminating between stages of PDAC malignancy. Therefore, we evaluated the performance of the combined microRNA-10b and -let7a markers and obtained excellent sensitivity and specificity for differentiating between PDAC, CP and NC with AUC >0.94 (**Figure 4i-m**). Importantly, the combined microRNAs differentiated between PDAC stages I & II and stages III & IV with 91% sensitivity and 87% specificity, better than the minimum sensitivity and specificity required to achieve cost effectiveness and prolong patient survival.[10] **Table 2** summarizes the performance metrics of individual and combined microRNAs as well as CA19-9 in distinguishing between the study cohorts.

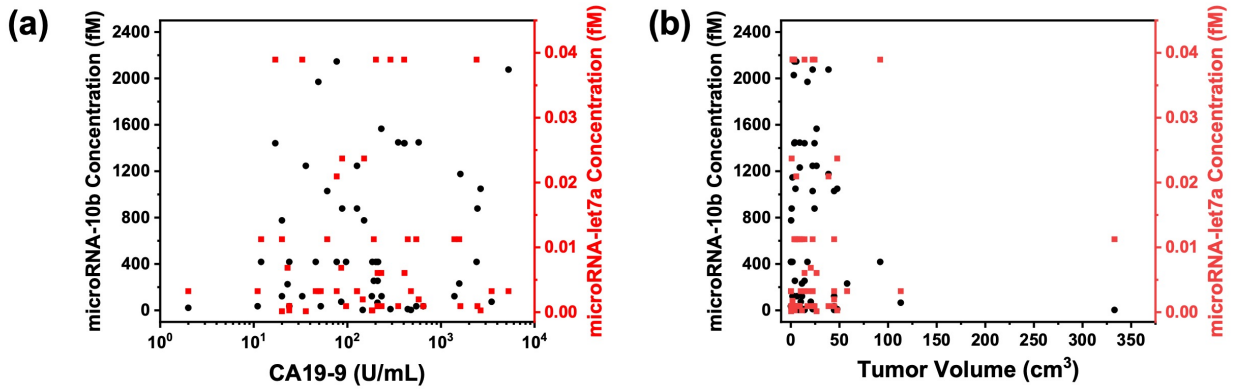

Figure 5. Comparison of nanoplasmonic sensor-based microRNA analyses with conventional clinical variables. (a,b) Correlation of PDAC microRNA-10b (black circles) and microRNA-let7a (red squares) signature values with serum CA19-9 concentrations and the tumor volume for 56 and 51 PDAC pre-surgery patients, respectively. The threshold value of CA19-9 for positive PDAC is 37 U/mL.

As shown in **Figure 5a**, we next determined whether nanoplasmonic sensor-based microRNA levels correlated with the clinical gold standard CA19-9 levels in PDAC patients. In our cohort, only 70% of PDAC patients (39 of 55, stages I-III) displayed an increased CA19-9 concentration (>37 U/mL, the clinical threshold value). We observed a slight correlation between microRNA-10b and CA19-9 levels (r = 0.21); however, there was no correlation between microRNA-let7a and CA19-9 (r = -0.06). Additionally, combining the microRNA biomarkers resulted in a slight increase in correlation with CA19-9 (**Supporting Figure S15**). The lack of strong correlation between the microRNA markers and CA19-9 is not surprising, given the superior performance of the microRNAs in predicting PDAC. Finally, analysis of the individual and combined microRNA levels versus tumor size showed no correlation between them (r = 0.01 or -0.16, r = 0.1594) (**Figure 5b, Supporting Figure S15**).

Discussion

One in seventy-one Americans will develop PDAC in their lifetime, and <10% of affected individuals will survive for more than five years post diagnosis.[79] Therefore, there is a substantial need to develop novel diagnostic tests to identify PDAC at an earlier stage to promote early cancer detection and prevention. Several pancreatic diseases, including CP, increase the risk of developing PDAC, and thus it is of paramount importance to develop highly sensitive and specific technology that can detect malignant progression in high-risk patient populations. The major

conclusion of this study is that an ultrasensitive assay for a combination of circulating oncogenic and tumor suppressor microRNAs can increase the sensitivity and specificity of a blood test for early stage PDAC diagnosis. One of the important features of our study design was that we specifically analyzed marker performance in patients with resectable early-stage PDAC (stages I & II) versus CP or controls to identify markers of malignant progression. Markers clearly correlating with disease progression from healthy or benign states can facilitate screening efforts by identifying patients at earlier stages amenable to resection. In the present study, we demonstrated that the level of elevated microRNA-10b returned to close to that of normal healthy controls within 3-5 days following PDAC resection ($p<0.0001$), suggesting concomitant normalization of microRNA levels in circulation following tumor removal (**Supporting Figure 16**). Therefore, the nanoplasmonic sensor-based assay has the potential to be used not only for diagnostics but also to monitor patient care following surgery and/or treatment utilizing microRNAs as prognostic biomarkers.

In the study cohort, our assay also showed that the selected microRNAs can differentiate between PDAC cancer grades. Importantly, we show that combining microRNA-10b and -let7a biomarkers provided ~91% sensitivity and above 87% specificity for differentiating between stage I & II versus stage III & IV whereas a single biomarker displayed <68% sensitivity (**Table 2**). Furthermore, the gold standard biomarker CA19-9 has limited sensitivity and specificity. Specifically, 27% of our cohort (15 of 55) did not express CA19-9 above the clinical threshold value (>37 U/mL) and conversely, ~26% CP patients (7 of 26) showed CA19-9 values >37 U/mL. Overall, in the present study, the combined biomarkers provided outstanding accuracy, above 98% sensitivity and 100% specificity at 95% CI, in distinguishing PDAC from CP, whereas CA19-9 alone cannot differentiate between PDAC and CP. Taken together, we believe that our nanoplasmonic assay can be used as a non-invasive and accurate liquid biopsy for early PDAC detection and help improve the patient survival rate from this deadly malignancy. Since it is possible that other diseases or conditions may provide false-positive results, testing more microRNAs[16, 31] along with a cohort of different cancers[80] would be necessary to further validate this technology for clinical use. Nevertheless, specificity, as high as 99%, is the key for any potential biofluid-based PDAC screening test.

MicroRNAs are short non-coding RNAs which are increasingly recognized as attractive circulating biomarkers for the clinical diagnosis and prognosis of cancer because of their unusually high stability in bodily fluids. Current microRNA analysis techniques lack high-throughput capability, require time consuming isolation procedures, and lack the sensitivity required for low abundance biomarkers, which together limits potential application in a clinical

setting. For example, qRT-PCR-based microRNA assay in pancreatic disease-associated plasma samples failed to differentiate between different stages of PDAC, between CP and normal controls,16 or produced varying results in case-controlled studies evaluating microRNA profiling in whole blood31 and plasma/serum.45 The nanoplasmonic sensor presented herein, by utilizing the LSPR properties of MNPs, specific geometric features, and novel sensing mechanism, allowed ultrasensitive detection and quantification of microRNAs in unprocessed patient plasma samples with exquisite sensitivity and specificity. The sensor fabrication strategy and assay are highly reproducible and affordable (**Supporting Figure 17)**. The multistep process described in Figure 1a is the standard approach for the fabrication of LSPR-based microRNA sensor. This high reproducibility of the method is due to reproducible synthesis of Au TNPs, as well as precautions that are taken during sensor fabrication steps. Specifically, we attach the Au TNP to the glass substrate with extreme precaution to make sure no damage to the sensing layer occurs through the whole process. The high-throughput nanoplasmonic sensor constructed here currently costs $0.92 per biomarker/well (384-well plate costs $13 for supplies and reagents including Au TNPs, and $342 for -ssDNAs and spacers). The majority of the current costs are mostly associated with manual manufacture of the sensor and functional -ssDNAs. Current limitations of our developed nanoplasmonic sensor are: (i) high cost of specifically designed -ssDNAs, (ii) over-night incubation of sensors in patient biofluids, and (iii) volume of plasma (10 μL) required per biomarker. We expect that further optimization and bulk production will improve the assay proficiency and reduce the cost.

Over the years, nanotechnology-based optical device fabrication has gained serious attention for earlier detection of PDAC because currently this disease has no cure; however, for very small and localized tumors, the five-year survival increases to almost 60%.[81] The advantage of nanostructured optical devices is that they do not require additional labelling ("label-free") for biomarker assays. Regarding the assay of exosomal proteins as potential biomarkers, several nanotechnology-based optical devices could differentiate between PDAC versus CP, and PDAC versus normal controls; however, there are some serious limitations of those technologies: (i) extensive sample processing to isolate exosomes for surface protein analysis, (ii) expensive and complicated device fabrication strategy, (iii) requirement for specialized instrument that is not widely available, (iv) lack of high-throughput capability and/or (v) below clinically acceptable specificity and sensitivity. The ultrasensitive and high-throughput nanoplasmonic sensor that we have developed does not require any plasma processing, utilizes a simple multi-well plate reader in the absorption mode for data collection, and has high specificity and sensitivity that are required for cost effectiveness. Together, our technology overcomes most of the limitations in existing

technologies that are a pre-requisite for the clinical analysis and diagnosis of PDAC. Despite all the advantages, there are a few limitations in our study. Firstly, we could not compare the performance of our nanoplasmonic sensor-based assay results with CA19-9 for PDAC versus normal controls because CA19-9 was unavailable for control patient cohorts. Second, individuals with PDAC, CP, and controls were not age-matched, therefore there could be a potential influence on data analysis and interpretation. Third, IPMN and obstructive jaundice were lacking in our study cohort which could influence the diagnostic accuracy of our assay. Fourth, in the study cohort, we had a limited number of Stage I PDAC patients; future validation involving a larger number of Stage I & II PDAC patients is required to accurately assess the performance of the nanoplasmonic sensor-based early diagnostic test. Finally, our current incubation time for capturing target microRNAs is significantly lengthy (~14 hr). Furthermore, ~3 hr assay time is required to collect LSPR spectra from all 384 wells. Together, the incubation and assay time are much longer than conventional PCR technique. However, we should mention that the PCR-based approach for microRNA detection requires total RNA extraction, labelling, and amplification steps that are time consuming and labor extensive.

Conclusions

In summary, we have demonstrated the successful design and fabrication of an amplification-free, nanotechnology-based, label-free optical sensor, which is capable of ultrasensitive detection and quantification of circulating microRNAs from patient plasma samples without any extensive sample processing. The enhanced LSPR sensitivity due to appropriate structural modifications of -ssDNA receptor structure enables patient samples to be highly diluted, resulting in significantly reduced non-specificity. This assay provides an eight order of magnitude linear dynamic range. This is particularly important since microRNA levels may vary greatly between PDAC, CP as well as different stages of PDAC, so it is advantageous to precisely detect and quantify microRNA levels over a large concentration range to monitor early signs of malignant progression. Based on the microRNA assays, the nanoplasmonic sensor represents a promising technology for precise earlier pancreatic cancer detection in the clinical setting. Our chosen two microRNAs when combined unequivocally distinguish individuals with PDAC from those with CP, and early- and late-stage PDAC. Our sensor fabrication strategy is highly customizable and thus can be readily transformed into a multiplexed sensor where many PDAC-associated microRNAs[16, 31, 44] can be included in a single assay by simply attaching appropriate receptors in the device construct. A pancreatic cancer signature panel could be developed for novel and early diagnostic tests, as well as for monitoring reoccurrence following resection and/or treatment for this deadly

malignancy. A large number of microRNA biomarkers have already been reported for the detection of numerous cancer types.[25-27] High-throughput and easily customizable nanoplasmonic sensors can be utilized for the detection of other cancers in a single instrument run including multiple microRNAs for each cancer type to increase sensitivity, specificity, and cost effectiveness.

Experimental Methods

Silanization of coverslips. 25 x 25 mm dimension glass coverslips (Fisher Scientific, 12548C) were functionalized according to our previously published procedure.82 Coverslips were sonicated in a 10% (v/v) RBS detergent (Thermo Scientific, PI27952) solution in 90 °C water for 15 min and then rinsed several times with nanopure water (Thermo Scientific Barnstead Nanopure system), followed by incubation in a 1:1 (v/v) hydrochloric acid: methanol solution for 30 min. Then, coverslips were rinsed several times with nanopure water and were placed in a vacuum oven at 60 °C overnight. The following day, coverslips were brought to room temperature and then incubated in a 15% (v/v) solution of (3-mercaptopropyl)-trimethoxysilane (MPTMS, Thermo Scientific, B23726) in N_2 purged ethanolic solution for 30 min. Coverslips were then sonicated in N_2 purged ethanol 3x for 15 min each time. After rinsing, coverslips were placed in the vacuum oven at 120 °C for a minimum of 3 hrs. The MPTMS-functionalized coverslips were stored in the vacuum oven up or at 4 °C up to one week for nanoplasmonic sensor fabrication.

Synthesis of gold triangular nanoprisms (Au TNPs). Au TNPs were chemically synthesized according to our previously published procedure with modifications.[82] Briefly, 10.4 mg (0.05 mmol) chloro(triethylphosphine) gold(I) (Et_3PAuCl, 97%, Gelest Inc, OMGO017) was dissolved in 20 mL of N_2 purged acetonitrile (CH_3CN, 99.9% ACS grade, Sigma Aldrich, A21-4) and allowed to stir for 5-10 min at room temperature. Then, 0.019 mL (0.273 mmol) of triethylamine (TEA, 99%, Sigma Aldrich, 471283) was added into the gold salt solution and heated on a hot plat to attain an internal temperature between 30-32 °C. After stirring for 30 min, 0.3 mL of poly(methylhydrosiloxane) (PMHS, Mn = 1700-3300, Sigma Aldrich, 176206) was added slowly and the reaction was allowed to proceed with gentle magnetic stirring. During the reaction, the color of the solution changed from clear to pink, light blue, dark navy blue, and then light purple. The reaction was continuously monitored until it was a dark purple color solution, indicating the formation of Au TNPs. Au TNPs display a stable localized surface plasmon resonance (LSPR) dipole peak (λ_{LSPR}) position at 800 or 850 nm for ~42 nm edge length or ~55 nm edge length Au TNPs respectively. When the solution displayed desired LSPR peak position associated to a particular dimension of Au TNPs, the solution was removed from heat and centrifuged at 7000 rpm for 10 sec. Finally, previously prepared MPTMS-functionalized coverslips were incubated in the Au TNP solution for 1 hr immediately after centrifugation. Next, Au TNP-attached coverslips were rinsed with acetonitrile to remove any loosely bound Au TNPs and were dried with N_2 flow. The Au TNP-attached coverslips were stored under N_2 at 4 °C for up to one week.

Fabrication of 384-well nanoplasmonic sensors. The 384-well plate-based nanoplasmonic sensors were constructed using our previously published procedure, with modification, as follows:[83] (1) MPTMS-functionalized coverslips were incubated in a freshly-synthesized Au TNP solution for one hour and then washed with ACN and dried with N_2 flow. (2) Au TNP-attached coverslips were tape cleaned to remove any non-prismatic nanostructures. Tape clean procedure is adapted from our previously published procedure.82 Briefly, the coverslip is placed on a granite block. 3 M scotch tape is gently pressed down onto the coverslip using a thumb and then gently lifted off at a 90° angle. (3) Tape-cleaned, Au TNP-attached coverslips were glued to the bottom of a no-bottom 384 well plate (Greiner Bio One, 781000-06). A small amount of glue was applied around the edges of the wells carefully, with one coverslip covering 25 wells (5 x 5 well area). The biosensor platform was allowed to dry for 1 hr at room temperature in dark. After 1 hr, each well in the biosensor platform was incubated in 0.120 mL nanopure water to check for leakage. After confirming no leakage, wells were incubated in 0.120 mL PBS buffer (pH = 7.2, prepared using RNAse free water (Fisher Scientific, 04-821-932) and the LSPR extinction spectra of each well was collected.

MicroRNA assay in healthy human plasma. After the fabrication of the 384-well construct, each well was incubated in a mixture of 0.120 mL of 1.0:1.0 μM solution of 3′-SH-$(CH_2)_3$-ssDNA-X: PEG_4-SH in PBS buffer overnight, where X = 10b, Super-10b, Amino-10b, Super-let7a. 3'-SH-$(CH_2)_3$-ssDNA-X was purchased from Integrated DNA technologies (IDT) and PEG_4-SH was purchased from purePEG (367404). Each well where Au TNPs were functionalized with -ssDNA: PEG_4-SH is denoted as independent nanoplasmonic sensor. Each sensor was rinsed several times with PBS buffer to remove any loosely adsorbed materials. The LSPR extinction spectra of each sensor were then collected in PBS buffer to determine the LSPR-wavelength maximum (λ_{LSPR}). Then, each sensor was incubated in 0.120 mL microRNA-X solution (IDT), here X= -10b or -let7a, at different concentrations, ranging from 100 nM to 1.0 aM in PBS buffer or 10% healthy human plasma overnight. Each sensor was rinsed several times with PBS buffer to remove any non-adsorbed microRNA-X and then LSPR extinction spectra of each biosensor were collected in PBS buffer to obtain the λ_{LSPR}. The change in λ_{LSPR} ($\Delta\lambda_{LSPR}$) was then calculated and calibration curves were developed by plotting $\Delta\lambda_{LSPR}$ verses concentration of microRNA-X in logarithm scale. False positive analyses were conducted by incubating sensors in 10% healthy human plasma without any complementary microRNAs. False negative analyses were conducted by incubating only PEG_4-SH functionalized Au TNP bound wells in 100 nM to 1.0 aM microRNA solutions in PBS.

Conditioned media from monolayer and 3D cell culture. Low passage patient-derived cells, Pa03C were plated in T-25 flasks for monolayer and in 6-well ultra-low adherence plates (Corning Inc., Life Sciences) for 3D culture. The media was DMEM+5%FBS for monolayer and DMEM+5%FBS+3% Reduced Growth Factor Matrigel for 3D spheroid cultures. $4x10^4$ cells were plated for the 3D assay and spheroids were allowed to form for four days before conditioned media was collected. 200 μL of cell culture medium was collected from monolayer and 3D cultures at timepoints indicated and then the media spun down at 2000 rpm for 5 min and immediately frozen and stored at -80.

Patient samples. Individuals with pancreatic cancer were treatment-naïve prior to undergoing resection. Diagnosis of pancreatic cancer or chronic pancreatitis as well as PDAC stage (TNM) and tumor size was obtained from the final pathology report. Patient variables such as age, sex, and serum CA19-9 values were retrieved from patient medical records. The study was approved by the Indiana University Institutional Review Board (Protocol # 1011003217 and 15053) and each subject signed informed consent. Approximately, 15-20 mL blood was collected into EDTA-coated tubes prior to surgery for the patient cohort and ~3-5 days following surgery for a subset of PDAC patients from whom pre-surgery blood was collected. Identical procedure was followed for collecting NC specimens that were quickly placed on ice or refrigerator (4 ^{0}C), promptly processed by centrifugation (1000 x g for 5 min). Plasma supernatants were aliquoted and stored at -80 ^{0}C. For the plasma samples in the validation cohort, a total of 17 participants were included in this study. Whole blood samples were obtained from 15 patients who were newly diagnosed with PDAC and treatment naïve and from two NC, and each patient provided signed informed consent. The blood samples included in this study were collected using sodium citrate tubes and processed within one hour of collection. Whole blood samples were centrifuged at 1500g for 15 minutes to separate the red blood cells and the platelet-rich plasma (PRP). The PRP was transferred to a clean Falcon tube and centrifuged again at 1500g for 15 minutes to remove any remaining blood cells and produce platelet-poor plasma (PPP). The PPP was aliquoted into 250 µL fractions, flash frozen in liquid nitrogen, and stored in -80°C.

RNA isolation and RT-qPCR. Frozen aliquots of plasma samples were thawed at room temperature and RNA was extracted from 250 µl of plasma using miRNeasy Serum/Plasma Kit (Qiagen, Cat ID# 217184, Germantown, MD, USA) following the manufacturer's protocol. After RNA extraction from plasma, microRNA-10b and microRNa-let7a levels were determined in individual assays by RT-qPCR. To assay the miRNA expression levels, a 4.0 uL RNA aliquot was reverse transcribed to cDNA using TaqMan Advanced miRNA cDNA Synthesis Kit (ThermoFisher Scientific, Cat ID# A28007, Waltham, MA). The expression levels of microRNA-10b and microRNa-let7a were determined using hsa-microRNA-10b-5p (Assay ID# 478494_miR) and hsa-microRNA-let7a-5p (Assay ID# 478575_miR) and normalized to microRNA-425-3p (hsa-miR-425-3p, Assay ID# 478093_mir). After normalization to microRNA-425-3p (ΔC_t), the ΔC_t values for microRNAs in normal controls were averaged and subtracted from the ΔC_t values of each individual PDAC sample ($\Delta\Delta C_t$). Fold changes of microRNA-10b and microRNa-let7a for each PDAC patient were calculated using normal controls as baseline using the $2^{-\Delta\Delta Ct}$ method.42, 43 All samples were run in triplicates.

Nanoplasmonic sensor-based patient sample assay. For nanoplasmonic sensor-based assay, stored plasma specimens were analyzed without any further sample processing. Sensors were incubated in a solution containing 10.0 µL of patient sample (PDAC pre-surgery, PDAC post-surgery, CP, or NC) diluted with 0.110 mL PBS buffer overnight. Sensors were then rinsed several times with PBS buffer to remove any loosely bound, unwanted endogenous biomolecules. LSPR extinction spectra were recorded and λ_{LSPR} was obtained. The experimentally determined λ_{LSPR} value was then put into the corresponding microRNA calibration curve equation developed in 10% healthy human plasma as "y" and the concentration of each microRNA was calculated by solving for "x".

Spectroscopy and other techniques. Absorption and extinction spectra in the range of 400−1050 nm were collected with a SpectraMax M5 microplate reader from Molecular Devices, LLC. Extinction spectra of Au TNP attached onto glass substrates were measured in air in order to determine the LSPR peak position (λ_{LSPR}). In the LSPR-based microRNA assays utilizing Au TNPs, all extinction spectra were recorded in PBS buffer. All extinction spectra were collected at room temperature. A silanized blank glass coverslip immersed in PBS buffer was used as a background. The chemically synthesized Au TNPs attached onto the silanized glass coverslips inside the multi-well plates were characterized using a JEOL 7800F scanning electron microscopy (SEM). Atomic force microscopy (AFM) images were acquired using Bruker Dimension 3000 instrument. The instrument was operated in tapping mode using beam shaped super sharp silicon cantilevers (SSS-NCHR, nanoANDmore) having an average force constant of 42 N/m. The operation frequency of the cantilevers for all measurements was 330 KHz.

Data processing and statistical analysis. The λ_{LSPR} was obtained by using the maxima of the UV-visible extinction spectra which was determined through curve fitting using Origin software. $\Delta\lambda_{LSPR}$ was determined by taking the difference between the λ_{LSPR} of sensors before and after hybridization with the target microRNA. Calibration curves were constructed by plotting $\Delta\lambda_{LSPR}$ vs microRNA concentration, with concentration being plotted in logarithmic scale in order to investigate nonspecific adsorption at a lower concentration range. The calibration curve equation was determined through linear regression using Origin software. The limit of detection (LOD) was determined by plugging the Z value (Z = mean of blank + 3 σ, σ = standard deviation of blank) into the calibration curve equation as “y” and solving for “x”. Concentration of microRNAs in patient samples was determined from the calibration curves developed in 10% healthy human plasma with $\Delta\lambda_{LSPR}$ representing the average of three measurements. Limit of quantification (LOQ) was determined by plugging in the value obtained from Z =mean of blank + 10 σ (standard deviation of blank) into the calibration curve equation as “y” and solving for “x”. Non-parametric one-way ANOVA, Wilcoxon t test, and area under the curve (AUC) of the receiver operating characteristic (ROC) graphs were plotted using GraphPad Prism at the 95% confidence interval. P values represent: 0.1234 (ns), 0.0332 (*), 0.0021 (**), 0.0002 (***), and <0.0001 (****).

FDTD simulations. The FDTD simulations (Lumerical Solutions 8.0, Inc., Canada) was used to monitor the E-field distributions of the nanostructure based on Maxwell’s equations. During the simulation, the dielectric constant of gold was taken from Johnson and Christy’s database provided in the software. Water was used as the surrounding environment (n = 1.33) and the mesh size was set to 0.5 nm in all spatial dimensions. A Total-field scattered-field source with a wavelength range from 400 to 1600 nm was launched into the box containing target objects. A perfectly matched layer (PML) boundary condition was applied to all the directions. A frequency-domain field and power monitor were placed in XY plane to visualize E-field distributions of the TNP.

Acknowledgements
This work was primarily supported by research funding provided by NSF grant (CBET-1604617 and 2204681). We also thank IUPUI-OVCR for financial support. M.L.F. was supported by grants from the National Institute of Health and National Cancer Institute R01CA167291,

R01CA254110, and U01HL143403. M.L.F. was additionally supported by the Riley Children's Foundation and the IU Simon Comprehensive Cancer Center (IUSCCC), P30CA082709. We would like to acknowledge IUSM Pathology Core and Dr. George Sandusky, Megan Szymanski, and Maggie Granatir with their help with the pictures and pathology of the patient samples. We thank the IUSCCC for the use of the Tissue Procurement & Distribution Core, which provided the tissue and blood samples for the validation cohort and the IUSCCC for the support of Pancreatic Cancer working group for sample procurement.

Author contributions

R.S. conceived the original idea. A.N.M. and R.S. designed the research plan. A.N.M. performed all the LSPR-related experiments and corresponding data analysis. N.N.C and M.L.F. prepared cell conditioned media and performed PCR analysis. A.N.M, Y.F. and S.C. conducted statistical analysis. M.T.Y.-S., H.W., and C.M.S. collected and processed the clinical samples in this study and retrieved patient data. S.H. performed DFT and FDTD calculations. P.G. performed the AFM analysis. A.N.M., N.N.C., M.T.Y.-S., M.L.F., and R.S. co-wrote the manuscript, and other authors contributed to reviewing and editing the manuscript.

Supporting Information. Additional SEM and AFM images of Au TNPs, extinction spectra of Au TNPs, calibration plots for microRNAs, binding isotherm, p-value graphs, microRNA quantification plots, ROC/AUC graphs, reproducibility studies, and tables for microRNA sequences, limit of detection values, and dipole moments.

References

1. Beatty, G. L.; Werba, G.; Lyssiotis, C. A.; Simeone, D. M. The biological underpinnings of therapeutic resistance in pancreatic cancer. *Genes & Dev.* **2021**, 1-23.
2. Ryan, D. P.; Hong, T. S.; Bardeesy, N. Pancreatic adenocarcinoma. *N Engl J Med* **2014**, *371*, 1039-1049.
3. Kleeff, J.; Korc, M.; Apte, M.; La Vecchia, C.; Johnson, C. D.; Biankin, A. V.; Neale, R. E.; Tempero, M.; Tuveson, D. A.; Hruban, R. H.*, et al.* Pancreatic cancer. *Nat Rev Dis Primers* **2016**, *2*, 16022.
4. Tsuchiya, R.; Noda, T.; Harada, N.; Miyamoto, T.; Tomioka, T.; Yamamoto, K.; Yamaguchi, T.; Izawa, K.; Tsunoda, T.; Yoshino, R.*, et al.* Collective review of small carcinomas of the pancreas. *Ann Surg* **1986**, *203*, 77-81.
5. Ansari, D.; Bauden, M.; Bergström, S.; Rylance, R.; Marko-Varga, G.; Andersson, R. Relationship between tumour size and outcome in pancreatic ductal adenocarcinoma. *Br J Surg* **2017**, *104*, 600-607.
6. Egawa, S.; Takeda, K.; Fukuyama, S.; Motoi, F.; Sunamura, M.; Matsuno, S. Clinicopathological aspects of small pancreatic cancer. *Pancreas* **2004**, *28*, 235-240.
7. Rahib, L.; Smith, B. D.; Aizenberg, R.; Rosenzweig, A. B.; Fleshman, J. M.; Matrisian, L. M. Projecting Cancer Incidence and Deaths to 2030: The Unexpected Burden of Thyroid, Liver, and Pancreas Cancers in the United States. *Cancer Research* **2014**, *74*, 2913-2921.
8. Menini, S.; Iacobini, C.; Vitale, M.; Pesce, C.; Pugliese, G. Diabetes and Pancreatic Cancer—A Dangerous Liaison Relying on Carbonyl Stress. *Cancers* **2021**, *13*, 313.
9. Steinberg, W. M.; Gelfand, R.; Anderson, K. K.; Glenn, J.; Kurtzman, S. H.; Sindelar, W. F.; Toskes, P. P. Comparison of the sensitivity and specificity of the CA19-9 and carcinoembryonic antigen assays in detecting cancer of the pancreas. *Gastroenterology* **1986**, *90*, 343-349.
10. Ghatnekar, O.; Andersson, R.; Svensson, M.; Persson, U.; Ringdahl, U.; Zeilon, P.; Borrebaeck, C. A. K. Modelling the benefits of early diagnosis of pancreatic cancer using a biomarker signature. *International Journal of Cancer* **2013**, *133*, 2392-2397.
11. Staal, B.; Liu, Y.; Barnett, D.; Hsueh, P.; He, Z.; Gao, C.; Partyka, K.; Hurd, M. W.; Singhi, A. D.; Drake, R. R.*, et al.* The sTRA Plasma Biomarker: Blinded Validation of Improved Accuracy Over CA19-9 in Pancreatic Cancer Diagnosis. *Clinical Cancer Research* **2019**, *25*, 2745-2754.
12. Galli, C.; Basso, D.; Plebani, M. CA 19-9: handle with care. *Clin Chem Lab Med* **2013**, *51*, 1369-1383.
13. Strijker, M.; Soer, E. C.; de Pastena, M.; Creemers, A.; Balduzzi, A.; Beagan, J. J.; Busch, O. R.; van Delden, O. M.; Halfwerk, H.; van Hooft, J. E.*, et al.* Circulating tumor DNA quantity is related to tumor volume and both predict survival in metastatic pancreatic ductal adenocarcinoma. *Int J Cancer* **2020**, *146*, 1445-1456.
14. Sivapalan, L.; Kocher, H. M.; Ross-Adams, H.; Chelala, C. Molecular profiling of ctDNA in pancreatic cancer: Opportunities and challenges for clinical application. *Pancreatology* **2021**, *21*, 363-378.
15. Tesfaye, A. A.; Azmi, A. S.; Philip, P. A. miRNA and Gene Expression in Pancreatic Ductal Adenocarcinoma. *Am J Pathol* **2019**, *189*, 58-70.
16. Cote, G. A.; Gore, J. A.; McElyea, S. D.; Heathers, L. E.; Xu, H.; Sherman, S.; Korc, M. A Pilot Study to Develop a Diagnostic Test for Pancreatic Ductal Adenocarcinoma Based on Differential Expression of Select miRNA in Plasma and Bile. *The American Journal of Gastroenterology* **2014**, *109*, 1942-1952.
17. Daoud, A. Z.; Mulholland, E. J.; Cole, G.; McCarthy, H. O. MicroRNAs in Pancreatic Cancer: biomarkers, prognostic, and therapeutic modulators. *BMC Cancer* **2019**, *19*, 1130.

18. Duell, E. J.; Lujan-Barroso, L.; Sala, N.; Deitz McElyea, S.; Overvad, K.; Tjonneland, A.; Olsen, A.; Weiderpass, E.; Busund, L. T.; Moi, L.*, et al.* Plasma microRNAs as biomarkers of pancreatic cancer risk in a prospective cohort study. *Int J Cancer* **2017**, *141*, 905-915.
19. Lindgaard, S. C.; Sztupinszki, Z.; Maag, E.; Chen, I. M.; Johansen, A. Z.; Jensen, B. V.; Bojesen, S. E.; Nielsen, D. L.; Hansen, C. P.; Hasselby, J. P.*, et al.* Circulating Protein Biomarkers for Use in Pancreatic Ductal Adenocarcinoma Identification. *Clinical Cancer Research* **2021**, *27*, 2592-2603.
20. Cohen, J. D.; Javed, A. A.; Thoburn, C.; Wong, F.; Tie, J.; Gibbs, P.; Schmidt, C. M.; Yip-Schneider, M. T.; Allen, P. J.; Schattner, M.*, et al.* Combined circulating tumor DNA and protein biomarker-based liquid biopsy for the earlier detection of pancreatic cancers. *Proceedings of the National Academy of Sciences* **2017**, *114*, 10202-10207.
21. Khoja, L.; Backen, A.; Sloane, R.; Menasce, L.; Ryder, D.; Krebs, M.; Board, R.; Clack, G.; Hughes, A.; Blackhall, F.*, et al.* A pilot study to explore circulating tumour cells in pancreatic cancer as a novel biomarker. *British Journal of Cancer* **2012**, *106*, 508-516.
22. Tjensvoll, K.; Nordgård, O.; Smaaland, R. Circulating tumor cells in pancreatic cancer patients: Methods of detection and clinical implications. *International Journal of Cancer* **2014**, *134*, 1-8.
23. Liang, K.; Liu, F.; Fan, J.; Sun, D.; Lyon Christopher, J.; Yokoi, K.; Liang, K.; Li, Y.; Liu, C.; Hu, Y.*, et al.* Nanoplasmonic Quantification of Tumor-derived Extracellular Vesicles in Plasma Microsamples for Diagnosis and Treatment Monitoring. *Nat Biomed Eng* **2017**, *1*.
24. Yang, K. S.; Im, H.; Hong, S.; Pergolini, I.; Fernandez del Castillo, A.; Wang, R.; Clardy, S.; Huang, C.-H.; Pille, C.; Ferrone, S.*, et al.* Multiparametric plasma EV profiling facilitates diagnosis of pancreatic malignancy. *Sci. Transl. Med.* **2017**, *9*, eaal3226/3221-eaal3226/3210.
25. Esquela-Kerscher, A.; Slack, F. J. Oncomirs - microRNAs with a role in cancer. *Nature Reviews Cancer* **2006**, *6*, 259-269.
26. Lin, S.; Gregory, R. I. MicroRNA biogenesis pathways in cancer. *Nature Reviews Cancer* **2015**, *15*, 321-333.
27. Lu, J.; Getz, G.; Miska, E. A.; Alvarez-Saavedra, E.; Lamb, J.; Peck, D.; Sweet-Cordero, A.; Ebert, B. L.; Mak, R. H.; Ferrando, A. A.*, et al.* MicroRNA expression profiles classify human cancers. *Nature* **2005**, *435*, 834-838.
28. Komatsu, S.; Ichikawa, D.; Hirajima, S.; Kawaguchi, T.; Miyamae, M.; Okajima, W.; Ohashi, T.; Arita, T.; Konishi, H.; Shiozaki, A.*, et al.* Plasma microRNA profiles: identification of miR-25 as a novel diagnostic and monitoring biomarker in oesophageal squamous cell carcinoma. *British Journal of Cancer* **2014**, *111*, 1614-1624.
29. Mitchell, P. S.; Parkin, R. K.; Kroh, E. M.; Fritz, B. R.; Wyman, S. K.; Pogosova-Agadjanyan, E. L.; Peterson, A.; Noteboom, J.; O'Briant, K. C.; Allen, A.*, et al.* Circulating microRNAs as stable blood-based markers for cancer detection. *Proceedings of the National Academy of Sciences* **2008**, *105*, 10513-10518.
30. Chen, X.; Ba, Y.; Ma, L.; Cai, X.; Yin, Y.; Wang, K.; Guo, J.; Zhang, Y.; Chen, J.; Guo, X.*, et al.* Characterization of microRNAs in serum: a novel class of biomarkers for diagnosis of cancer and other diseases. *Cell Research* **2008**, *18*, 997-1006.
31. Schultz, N. A.; Dehlendorff, C.; Jensen, B. V.; Bjerregaard, J. K.; Nielsen, K. R.; Bojesen, S. E.; Calatayud, D.; Nielsen, S. E.; Yilmaz, M.; Holländer, N. H.*, et al.* MicroRNA Biomarkers in Whole Blood for Detection of Pancreatic Cancer. *JAMA* **2014**, *311*, 392-404.
32. Nagarajan, M. B.; Tentori, A. M.; Zhang, W. C.; Slack, F. J.; Doyle, P. S. Nonfouling, Encoded Hydrogel Microparticles for Multiplex MicroRNA Profiling Directly from Formalin-Fixed, Paraffin-Embedded Tissue. *Anal. Chem.* **2018**, *90*, 10279-10285.
33. Cai, S.; Pataillot-Meakin, T.; Shibakawa, A.; Ren, R.; Bevan, C. L.; Ladame, S.; Ivanov, A. P.; Edel, J. B. Single-molecule amplification-free multiplexed detection of circulating microRNA cancer biomarkers from serum. *Nature Communications* **2021**, *12*, 3515.

34. Tang, L.; Li, J. Plasmon-Based Colorimetric Nanosensors for Ultrasensitive Molecular Diagnostics. *ACS Sensors* **2017**, *2*, 857-875.
35. Martins, C. S. M.; LaGrow, A. P.; Prior, J. A. V. Quantum Dots for Cancer-Related miRNA Monitoring. *ACS Sensors* **2022**, *7*, 1269-1299.
36. Wanunu, M.; Dadosh, T.; Ray, V.; Jin, J.; McReynolds, L.; Drndić, M. Rapid electronic detection of probe-specific microRNAs using thin nanopore sensors. *Nature Nanotechnology* **2010**, *5*, 807-814.
37. Dave, V. P.; Ngo, T. A.; Pernestig, A.-K.; Tilevik, D.; Kant, K.; Nguyen, T.; Wolff, A.; Bang, D. D. MicroRNA amplification and detection technologies: opportunities and challenges for point of care diagnostics. *Laboratory Investigation* **2019**, *99*, 452-469.
38. Willets, K. A.; Van Duyne, R. P. Localized surface plasmon resonance spectroscopy and sensing. *Annu. Rev. Phys. Chem.* **2007**, *58*, 267-297.
39. Mayer, K. M.; Hafner, J. H. Localized surface plasmon resonance sensors. *Chem. Rev. (Washington, DC, U. S.)* **2011**, *111*, 3828-3857.
40. Shamah, S. M.; Cunningham, B. T. Label-free cell-based assays using photonic crystal optical biosensors. *Analyst* **2011**, *136*, 1090-1102.
41. Fang, Y.; Ferrie, A. M.; Fontaine, N. H.; Mauro, J.; Balakrishnan, J. Resonant Waveguide Grating Biosensor for Living Cell Sensing. *Biophysical Journal* **2006**, *91*, 1925-1940.
42. Joshi, G. K.; Deitz-McElyea, S.; Liyanage, T.; Lawrence, K.; Mali, S.; Sardar, R.; Korc, M. Label-free nanoplasmonic-based short noncoding RNA sensing at attomolar concentrations allows for quantitative and highly specific assay of MicroRNA-10b in biological fluids and circulating exosomes. *ACS Nano* **2015**, *9*, 11075-11089.
43. Joshi, G. K.; Deitz-McElyea, S.; Johnson, M.; Mali, S.; Korc, M.; Sardar, R. Highly Specific Plasmonic Biosensors for Ultrasensitive MicroRNA Detection in Plasma from Pancreatic Cancer Patients. *Nano Lett.* **2014**, *14*, 6955-6963.
44. Lai, X.; Wang, M.; McElyea, S. D.; Sherman, S.; House, M.; Korc, M. A microRNA signature in circulating exosomes is superior to exosomal glypican-1 levels for diagnosing pancreatic cancer. *Cancer Lett. (N. Y., NY, U. S.)* **2017**, *393*, 86-93.
45. Liu, R.; Chen, X.; Du, Y.; Yao, W.; Shen, L.; Wang, C.; Hu, Z.; Zhuang, R.; Ning, G.; Zhang, C.*, et al.* Serum MicroRNA Expression Profile as a Biomarker in the Diagnosis and Prognosis of Pancreatic Cancer. *Clinical Chemistry* **2012**, *58*, 610-618.
46. Zheng, M.; Davidson, F.; Huang, X. Ethylene glycol monolayer protected nanoparticles for eliminating nonspecific binding with biological molecules. *J Am Chem Soc* **2003**, *125*, 7790-7791.
47. Liyanage, T.; Rael, A.; Shaffer, S.; Zaidi, S.; Goodpaster, J. V.; Sardar, R. Fabrication of a self-assembled and flexible SERS nanosensor for explosive detection at parts-per-quadrillion levels from fingerprints. *Analyst* **2018**, *143*, 2012-2022.
48. Hao, E.; Schatz, G. C. Electromagnetic fields around silver nanoparticles and dimers. *J. Chem. Phys.* **2004**, *120*, 357-366.
49. Otte, M. A.; Sepulveda, B.; Ni, W.; Perez Juste, J.; Liz-Marzan, L. M.; Lechuga, L. M. Identification of the Optimal Spectral Region for Plasmonic and Nanoplasmonic Sensing. *ACS Nano* **2010**, *4*, 349-357.
50. Liyanage, T.; Masterson, A. N.; Oyem, H. H.; Kaimakliotis, H.; Nguyen, H.; Sardar, R. Plasmoelectronic-Based Ultrasensitive Assay of Tumor Suppressor microRNAs Directly in Patient Plasma: Design of Highly Specific Early Cancer Diagnostic Technology. *Anal. Chem.* **2019**, *91*, 1894-1903.
51. Masterson, A. N.; Liyanage, T.; Kaimakliotis, H.; Gholami Derami, H.; Deiss, F.; Sardar, R. Bottom-Up Fabrication of Plasmonic Nanoantenna-Based High-throughput Multiplexing Biosensors for

Ultrasensitive Detection of microRNAs Directly from Cancer Patients' Plasma. *Analytical Chemistry* **2020**, *92*, 9295-9304.
52. Nath, N.; Chilkoti, A. Label-Free Biosensing by Surface Plasmon Resonance of Nanoparticles on Glass: Optimization of Nanoparticle Size. *Analytical Chemistry (Washington, DC, United States)* **2004**, *76*, 5370-5378.
53. Liyanage, T.; Sangha, A.; Sardar, R. Achieving biosensing at attomolar concentrations of cardiac troponin T in human biofluids by developing a label-free nanoplasmonic analytical assay. *Analyst* **2017**, *142*, 2442-2450.
54. Mayer, K. M.; Hafner, J. H. Localized surface plasmon resonance sensors. *Chemical Reviews (Washington, DC, United States)* **2011**, *111*, 3828-3857.
55. Willets, K. A.; Duyne, R. P. V. Localized Surface Plasmon Resonance Spectroscopy and Sensing. *Annual Rev. Phys. Chem.* **2007**, *58*, 267-297.
56. Haes, A. J.; Van Duyne, R. P. A Nanoscale Optical Biosensor: Sensitivity and Selectivity of an Approach Based on the Localized Surface Plasmon Resonance Spectroscopy of Triangular Silver Nanoparticles. *J. Am. Chem. Soc.* **2002**, *124*, 10596-10604.
57. Murphy, C. J.; Arkin, M. R.; Jenkins, Y.; Ghatlia, N. D.; Bossmann, S. H.; Turro, N. J.; Barton, J. K. Long-Range Photoinduced Electron Transfer Through a DNA Helix. *Science* **1993**, *262*, 1025-1029.
58. Wu, K.; Chen, J.; McBride, J. R.; Lian, T. Efficient hot-electron transfer by a plasmon-induced interfacial charge-transfer transition. *Science* **2015**, *349*, 632-635.
59. Foerster, B.; Spata, V. A.; Carter, E. A.; Sönnichsen, C.; Link, S. Plasmon damping depends on the chemical nature of the nanoparticle interface. *Science Advances* **2019**, *5*, eaav0704.
60. Gooding, J. J. What Does Ultrasensitive Really Mean? *ACS Sensors* **2019**, *4*, 528-528.
61. Xue, T.; Liang, W.; Li, Y.; Sun, Y.; Xiang, Y.; Zhang, Y.; Dai, Z.; Duo, Y.; Wu, L.; Qi, K.*, et al.* Ultrasensitive detection of miRNA with an antimonene-based surface plasmon resonance sensor. *Nature Communications* **2019**, *10*, 28.
62. Zhang, L.; Zhang, Y.; Hu, Y.; Fan, Q.; Yang, W.; Li, A.; Li, S.; Huang, W.; Wang, L. Refractive index dependent real-time plasmonic nanoprobes on a single silver nanocube for ultrasensitive detection of the lung cancer-associated miRNAs. *Chemical Communications* **2015**, *51*, 294-297.
63. Zhang, L.; Wang, J.; Zhang, J.; Liu, Y.; Wu, L.; Shen, J.; Zhang, Y.; Hu, Y.; Fan, Q.; Huang, W.*, et al.* Individual Au-Nanocube Based Plasmonic Nanoprobe for Cancer Relevant MicroRNA Biomarker Detection. *ACS Sensors* **2017**, *2*, 1435-1440.
64. Soares, L.; Csáki, A.; Jatschka, J.; Fritzsche, W.; Flores, O.; Franco, R.; Pereira, E. Localized surface plasmon resonance (LSPR) biosensing using gold nanotriangles: detection of DNA hybridization events at room temperature. *Analyst* **2014**, *139*, 4964-4973.
65. Miti, A.; Thamm, S.; Müller, P.; Csáki, A.; Fritzsche, W.; Zuccheri, G. A miRNA biosensor based on localized surface plasmon resonance enhanced by surface-bound hybridization chain reaction. *Biosensors and Bioelectronics* **2020**, *167*, 112465.
66. Pang, Y.; Wang, C.; Lu, L.; Wang, C.; Sun, Z.; Xiao, R. Dual-SERS biosensor for one-step detection of microRNAs in exosome and residual plasma of blood samples for diagnosing pancreatic cancer. *Biosensors and Bioelectronics* **2019**, *130*, 204-213.
67. Lee, J. U.; Kim, W. H.; Lee, H. S.; Park, K. H.; Sim, S. J. Quantitative and Specific Detection of Exosomal miRNAs for Accurate Diagnosis of Breast Cancer Using a Surface-Enhanced Raman Scattering Sensor Based on Plasmonic Head-Flocked Gold Nanopillars. *Small* **2019**, *15*, 1804968.
68. Su, Q.; Vogt, S.; Nöll, G. Langmuir Analysis of the Binding Affinity and Kinetics for Surface Tethered Duplex DNA and a Ligand–Apoprotein Complex. *Langmuir* **2018**, *34*, 14738-14748.

69. Goobes, R.; Kahana, N.; Cohen, O.; Minsky, A. Metabolic Buffering Exerted by Macromolecular Crowding on DNA−DNA Interactions: Origin and Physiological Significance. *Biochemistry* **2003**, *42*, 2431-2440.
70. Kumar, S.; Xue, L.; Arya, D. P. Neomycin−Neomycin Dimer: An All-Carbohydrate Scaffold with High Affinity for AT-Rich DNA Duplexes. *Journal of the American Chemical Society* **2011**, *133*, 7361-7375.
71. Nath, N.; Chilkoti, A. Label-Free Biosensing by Surface Plasmon Resonance of Nanoparticles on Glass: Optimization of Nanoparticle Size. *Analytical Chemistry* **2004**, *76*, 5370-5378.
72. Haes, A. J.; Hall, W. P.; Chang, L.; Klein, W. L.; Van Duyne, R. P. A Localized Surface Plasmon Resonance Biosensor: First Steps toward an Assay for Alzheimer's Disease. *Nano Letters* **2004**, *4*, 1029-1034.
73. Anonymous For the calculations of dipole moment and polarizability, first-principle density functional theory (DFT) calculation was carried out for each of the free -ssDNA systems with and without and Au atom at the BP86 and B3LYP functional level respectively in the Gaussian 16 program. The LANL2DZ basis set was used for the W atom and the 6-311+ G(d,p) basis set for the other atoms. The optimized structures were visualized by using Gaussview.
74. Sempere, L. F.; Powell, K.; Rana, J.; Brock, A. A.; Schmittgen, T. D. Role of non-coding RNAs in tumor progression and metastasis in pancreatic cancer. *Cancer Metastasis Rev* **2021**, *40*, 761-776.
75. Ouyang, H.; Gore, J.; Deitz, S.; Korc, M. microRNA-10b enhances pancreatic cancer cell invasion by suppressing TIP30 expression and promoting EGF and TGF-β actions. *Oncogene* **2014**, *33*, 4664-4674.
76. Torrisani, J.; Bournet, B.; du Rieu, M. C.; Bouisson, M.; Souque, A.; Escourrou, J.; Buscail, L.; Cordelier, P. let-7 MicroRNA transfer in pancreatic cancer-derived cells inhibits in vitro cell proliferation but fails to alter tumor progression. *Hum Gene Ther* **2009**, *20*, 831-844.
77. Lai, X.; Wang, M.; McElyea, S. D.; Sherman, S.; House, M.; Korc, M. A microRNA signature in circulating exosomes is superior to exosomal glypican-1 levels for diagnosing pancreatic cancer. *Cancer Lett* **2017**, *393*, 86-93.
78. Logsdon, D. P.; Shah, F.; Carta, F.; Supuran, C. T.; Kamocka, M.; Jacobsen, M. H.; Sandusky, G. E.; Kelley, M. R.; Fishel, M. L. Blocking HIF signaling via novel inhibitors of CA9 and APE1/Ref-1 dramatically affects pancreatic cancer cell survival. *Sci Rep* **2018**, *8*, 13759.
79. Siegel, R. L.; Miller, K. D.; Fuchs, H. E.; Jemal, A. Cancer statistics, 2022. *CA: A Cancer Journal for Clinicians* **2022**, *72*, 7-33.
80. Cohen, J. D.; Li, L.; Wang, Y.; Thoburn, C.; Afsari, B.; Danilova, L.; Douville, C.; Javed, A. A.; Wong, F.; Mattox, A.*, et al.* Detection and localization of surgically resectable cancers with a multi-analyte blood test. *Science* **2018**, *359*, 926-930.
81. Ansari, D.; Bauden, M.; Bergström, S.; Rylance, R.; Marko-Varga, G.; Andersson, R. Relationship between tumour size and outcome in pancreatic ductal adenocarcinoma. *British Journal of Surgery* **2017**, *104*, 600-607.
82. Joshi, G. K.; McClory, P. J.; Muhoberac, B. B.; Kumbhar, A.; Smith, K. A.; Sardar, R. Designing Efficient Localized Surface Plasmon Resonance-Based Sensing Platforms: Optimization of Sensor Response by Controlling the Edge Length of Gold Nanoprisms. *J. Phys. Chem. C* **2012**, *116*, 20990-21000.
83. Masterson, A. N.; Liyanage, T.; Kaimakliotis, H.; Gholami Derami, H.; Deiss, F.; Sardar, R. Bottom-Up Fabrication of Plasmonic Nanoantenna-Based High-throughput Multiplexing Biosensors for Ultrasensitive Detection of microRNAs Directly from Cancer Patients' Plasma. *Anal. Chem. (Washington, DC, U. S.)* **2020**, *92*, 9295-9304.

LIST OF TABLES

Table 1. Summary of validation and study cohorts

Characteristic	Validation Cohort	Study cohort		Total
	Patient	Patient	Control	
Total Cases (n)	15	110	60	185
Patient groups				
PDAC pre-surgery	-	75	-	75
PDAC post-surgery	-	75 (same as pre-surgery patients)	-	75 (same as pre-surgery patients)
CP	-	35	-	35
Age (years)				
Median	76	65	56	-
Range	46-88	18-90	39-80	-
Sex				
Male	7	63	29	99
Female	8	47	31	86
Stage				
I	1	5	-	6
II	6	29	-	35
III	8	29	-	37
IV	0	11	-	11

Table 2. Performance of microRNA-10b and microRNA-let7a (individual, combined) and CA19-9 in distinguishing between patient and control cohorts.[a,b,c]

		AUC (95% CI)	Cutoff	Sensitivity (%) (95% CI)	Specificity (%) (95% CI)
PDAC versus NC	microRNA-10b microRNA-let7a	1.00 (1.00-1.00) 1.00 (1.00-1.00)	>0.03227 <54.06	100 (95-100) 100 (95-100)	98.33 (91-100) 98.33 (91-100)
PDAC versus CP	microRNA-10b microRNA-let7a CA19-9	0.9890 (0.9763-1.00) 0.9943 (0.9856-1.00) 0.8088 (0.7072-0.9104)	>8.182 <0.08694 >19.00	94.29 (81-99) 94.29 (81-99) 41.67 (24-61)	94.67 (87-98) 98.67 (93-100) 92.16 (82-97)
Stages I & II PDAC versus NC	microRNA-10b microRNA-let7a	1.00 (1.00-1.00) 1.00 (1.00-1.00)	>0.03227 <54.06	100 (90-100) 100 (90-100)	98.33 (91-100) 98.33 (91-100)
Stages I & II PDAC versus CP	microRNA-10b microRNA-let7a CA19-9	0.9672 (0.9343-1.00) 0.9840 (0.9613-1.00) 0.7682 (0.6322-0.9043)	>8.182 <0.08694 >16.50	82.35 (66-92) 97.06 (85-100) 29.17 (15-49)	94.29 (81-99) 94.29 (81-99) 95.83 (80-100)
Stage I & II PDAC versus Stage III & IV PDAC	microRNA-10b microRNA-let7a CA19-9	0.8610 (0.7633-0.9587) 0.8180 (0.7155-0.9205) 0.6420 (0.4876-0.7964)	<1343 >0.001457 <319.5	62.5 (47-76) 67.50 (52-80) 44.44 (28-63)	88.24 (73-95) 76.47 (60-88) 83.33 (64-93)
PDAC versus NC	combined	1.00 (1.00-1.00)	>1.1526	100 (94-100)	100 (93-100)
PDAC versus CP	combined	1.00 (1.00-1.00)	<1.1526	98.67 (92-100)	100 (88-100)
Stages I & II PDAC versus NC	combined	1.00 (1.00-1.00)	>0.8473	100 (87-100)	100 (93-100)
Stages I & II PDAC versus CP	combined	0.9975 (0.9854-1.00)	<0.9445	97.06 (83-100)	100 (88-100)
Stage I & II PDAC versus Stage III & IV PDAC	combined	0.9449 (0.8884-1.00)	-0.4895	91.18 (75-98)	87.5 (72-95)

[a]Ninety-five percent CIs are indicated in parentheses. [b]All PDAC samples are pre-surgery plasma specimens. [c]Optimum cut-offs were determined by Youden Index.
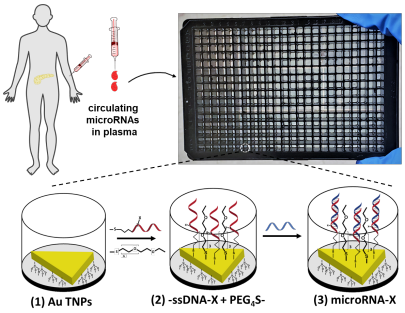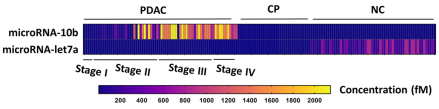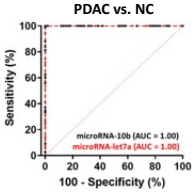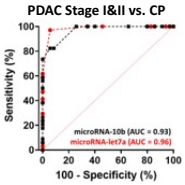
TOC Graphics